NREL/TP-451-7047 • UC Category: 273 • DE94011849

Role of Polycrystallinity in CdTe and $CuInSe_2$ Photovoltaic Cells

Final Subcontract Report
1 April 1990 – 30 November 1993

J. R. Sites
Colorado State University
Fort Collins, Colorado

NREL technical monitor: B. von Roedern

National Renewable Energy Laboratory
1617 Cole Boulevard
Golden, Colorado 80401-3393
A national laboratory of the U.S. Department of Energy
Managed by Midwest Research Institute
for the U.S. Department of Energy
under contract No. DE-AC36-83CH10093

Prepared under Subcontract No. XC-0-10046-1

July 1994

NOTICE

Available to DOE and DOE contractors from:
Office of Scientific and Technical Information (OSTI)
P.O. Box 62
Oak Ridge, TN 37831
Prices available by calling (615) 576-8401

Available to the public from:
National Technical Information Service (NTIS)
U.S. Department of Commerce
5285 Port Royal Road
Springfield, VA 22161
(703) 487-4650

Printed on paper containing at least 50% wastepaper and 10% postconsumer waste

DISCLAIMER

Portions of this document may be illegible electronic image products. Images are produced from the best available original document.

SUMMARY

Several aspects of the role of polycrystallinity in the operation of CdTe, $CuInSe_2$, and $Cu(In,Ga)Se_2$ solar cells have been explored. The work has included the refinement of several analytical techniques, the documentation and understanding of time-dependent voltage effects, the analysis of a large number of individual cells, and significant progress towards a viable current-voltage model. This work has been integral to the doctoral training of four students and has been greatly assisted by several active collaborations within the polycrystalline thin-film solar cell community.

TABLE OF CONTENTS

FIGURES

TABLES

INTRODUCTION

The objective of the Colorado State program is the quantitative evaluation of individual losses in thin-film polycrystalline solar cells. The primary focus areas during the past 3½ years have been: (1) The refinement of analytical techniques including incorporation of the voltage dependence of photocurement, capacitance for carrier density profiles, and the changes in individual parameters during annealing processes. (2) The characterization and explanation of time-dependent voltage effects. (3) The analysis of specific CdTe, $CuInSe_2$, and $Cu(In,Ga)Se_2$ cells. (4) Development of a current-voltage model consistent with observed variations with temperature and illumination.

Four research students, Rick Sasala, Xiaoxiang Liu, Ingrid Eisgruber, and Jennifer Granata, plus visiting scientist John Scofield, have been responsible for much of the experimental and analytical work. Rick Sasala completed his Ph.D. in November 1993 and is now employed by Solar Cells, Inc. Xiaoxiang Liu has entered the thesis writing stage of her doctoral work.

The Colorado State program benefits considerably from active collaborations with a number of other laboratories. During the subcontract period, the major collaborations have been with the Institute of Energy Conversion, International Solar Energy Technology, Inc., the National Renewable Energy Laboratory, Solar Cells, Inc., and the University of South Florida. Other productive interactions have included Boeing, the Colorado School of Mines, the EUROCIS collaboration, Georgia Tech, Golden Photon, Martin Marietta, Oberlin College, Siemens Solar, Solarex, and the University of Toledo.

ANALYSIS TECHNIQUES

Collection Efficiency

The internal collection efficiency of a solar cell must be close to unity in the operating voltage range for a cell to be competitive. In general it is desirable to have a wide depletion region so that the electric field will assure that a large fraction of photocarriers are collected. This criterion is particularly important with thin-film cells where collection by diffusion is often limited by grain-boundary recombination and the physical thickness of the film. Wide depletion, however, often implies a low doping density and thus a small junction potential barrier and reduced voltage output [1]. Additionally, since depletion width changes with bias, the collection efficiency at operating voltages may be lower than that commonly measured under short circuit conditions. Even if such a reduction is modest, it can complicate the analysis of current-voltage curves [2].

The approximate collection efficiency for direct-gap cells, calculated as a function of depletion width is shown in Fig. 1. The corresponding hole density of a p-type absorber is shown at the top. The calculation assumes a typical variation of absorption coefficient with energy relative to the bandgap, and it assumes a standard solar spectrum [3]. It also assumes that collection efficiency in the depletion region is unity so long as the field-driven transit time is less than the recombination time. Collection from photons absorbed beyond the depletion region, however, will always be less than unity and will depend strongly on the effective depletion length L_{eff}. For hole densities above 10^{16} cm^{-2}, typical of $CuInSe_2$ cells, the reduction in collection efficiency can be significant. For densities below 10^{15} cm^{-2}, typical of CdTe, essentially all absorption takes place in the field-driven region, and internal collection efficiency should be close to unity.

If a positive voltage is applied to a solar cell, the depletion width, and hence the collection efficiency, will decrease, though often by only a small amount. Following the same procedure as with Fig. 1, but assuming parameters specific to different materials, the voltage-dependence

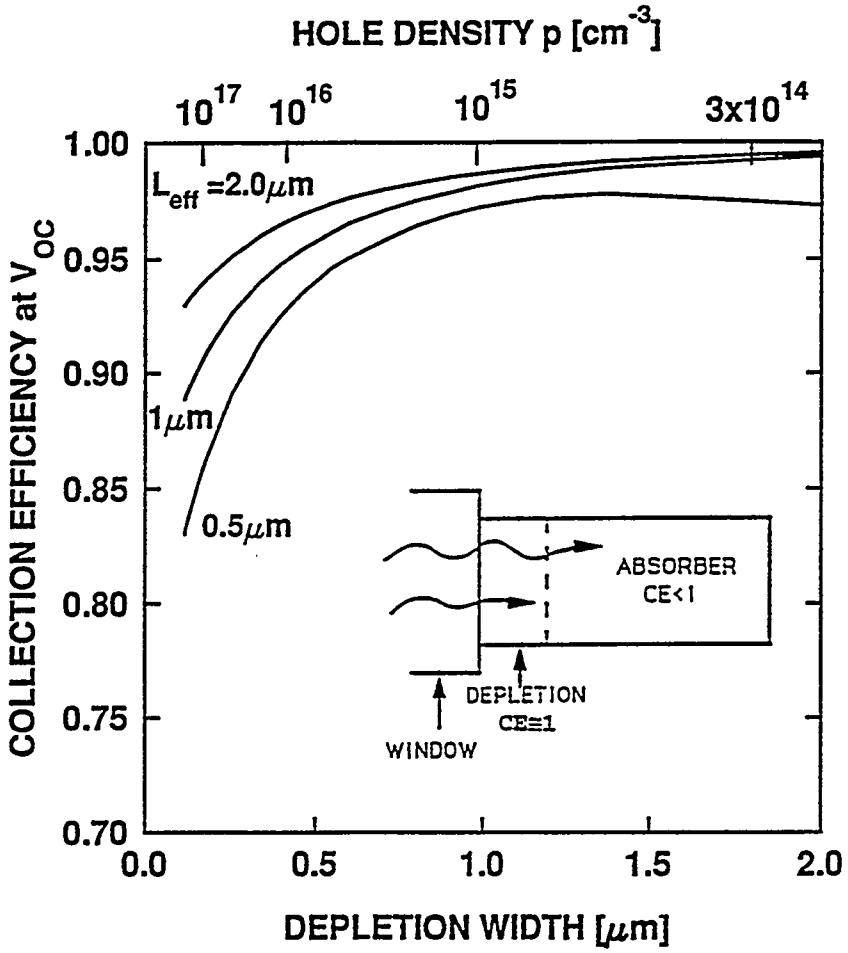

Figure 1. Calculated collection efficiency of typical direct-gap cells as a function of depletion width.

of photocurrents for four types of cell is calculated and shown in Fig. 2. The largest variation occurs for thin-film polycrystalline $CuInSe_2$, which has a photocurrent difference between zero and open-circuit voltage (~0.5 V) of about 3%. The expanded-scale inset shows that the photocurrent vs. voltage plot has considerable curvature, and hence need not be mistaken for a shunting effect, which should be more linear. For the crystalline Si cell, with its very large minority-carrier diffusion length (over 100 times that of polycrystalline $CuInSe_2$), the variation is essentially zero.

The effect of the voltage-dependent photocurrent on the forward current curve for a high-efficiency (13.2%) $CuInSe_2$ cell fabricated at NREL [4] is shown in Fig. 3. The open circles

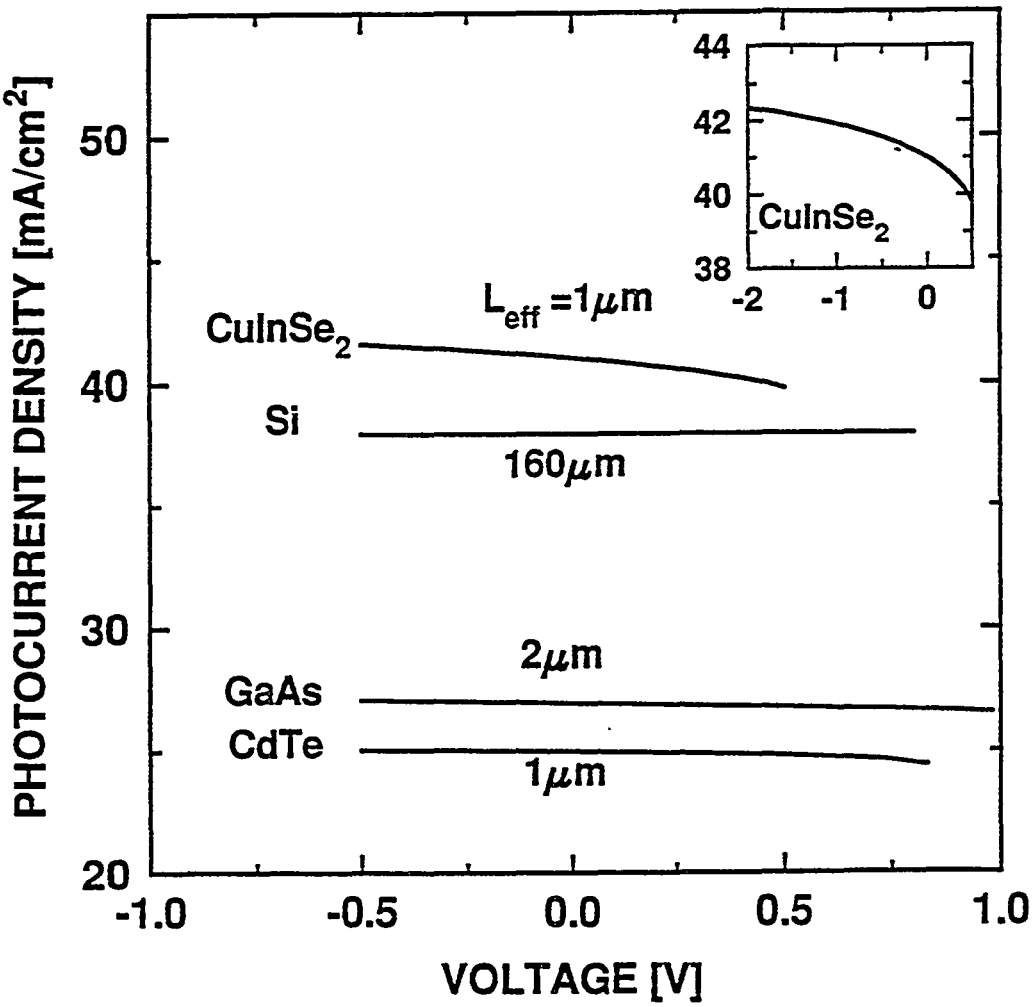

Figure 2. **Voltage-dependent photocurrents for four types of solar cells with typical doping densities. Curves are terminated at open-circuit voltage.**

show the forward current $J+J_L$, where the photocurrent J_L is assumed to be constant and equal to J_{sc}. The open triangle uses reasonable parameter estimates to calculate the voltage-dependent photocurrent $J_L(V)$. The correction yields a much more exponential current-voltage curve and one that is very nearly coincident with the dark data.

In terms of analysis, the $J_L(V)$ correction will have only a minor effect on extracting values for diode quality factor and series resistance. It will have a major effect, however, on deducing the shunt resistance. In the example shown, neglect of the $J_L(V)$ correction yields a shunt resistance near 3 $k\Omega\text{-}cm^2$. Inclusion leads to a value at least ten times larger.

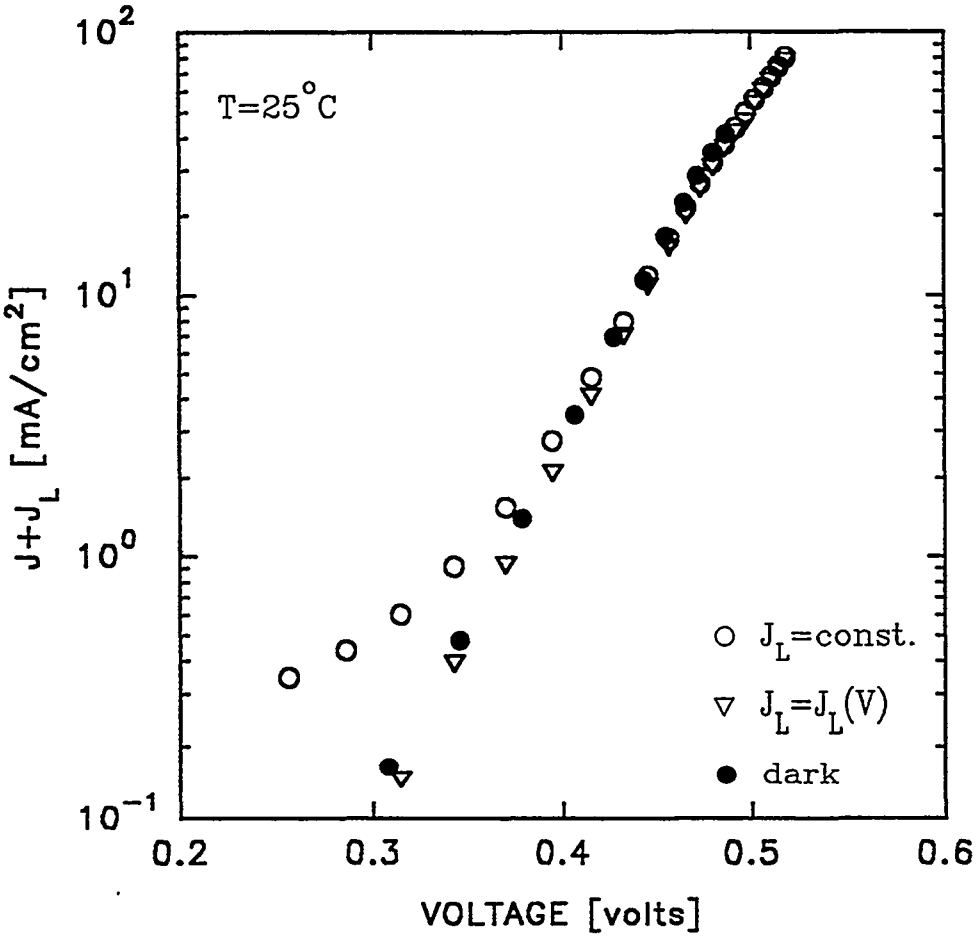

Figure 3. Forward current under illumination for NREL $CuInSe_2$ cell M1201-14#4 comparing constant and voltage-dependent photocurrent assumptions. Dark data shown for reference.

A general summary of the magnitude of the predicted reduction in photocurrent with voltage is given in Fig. 4. Here W_o is depletion width at zero voltage and $<\alpha>$ is an average absorption coefficient, which corresponds to absorption near the maximum intensity of the solar spectrum. Two different minority-carrier diffusion lengths and two voltages are shown. For polycrystalline thin-film cells, $V/V_{bi}=0.5$ is generally near the maximum-power voltage. For good crystalline cells, the ratios of these voltages to the built-in potential may be slightly higher. Fig. 4 shows that larger voltages and smaller diffusion lengths correspond to larger changes in photocurrent. It also shows that the greatest effect occurs when the most light is absorbed in the spatial region that changes from depletion to bulk with increasing voltage, or more mathematically, when the product [1,2] of absorption coefficient and depletion width is close to one.

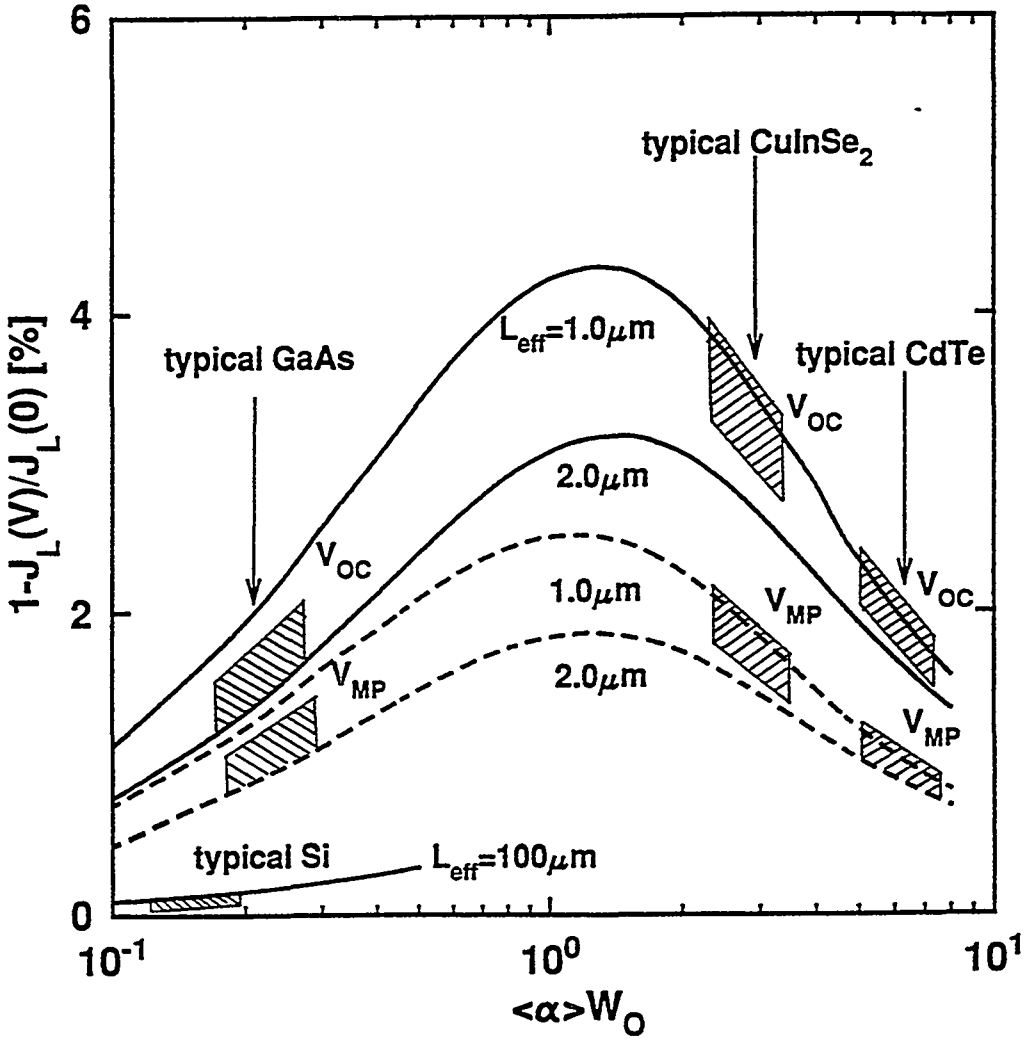

Figure 4. **Calculated magnitude of photocurrent reduction with voltage. Solid curves are for $V = 0.7V_{bi}$, which should be near V_{oc}. Dashed curves are for $V = 0.5\ V_{bi}$, which is generally near V_{mp}.**

The conclusions from Fig. 4 are equivalent to the curves shown earlier in Fig. 2. For good-quality $CuInSe_2$ cells, $<\alpha>W_o$ is often not far from unity, and the reduction in photocurrent may be significant (3½% at V_{oc} near 500 mV and $L_{eff} = 1\ \mu m$). CdTe cells, in contrast, tend to have larger depletion regions, which can be determined directly through capacitance measurements [5]. In many cases the entire CdTe layer ($\sim 2\ \mu m$) is depleted, and the cell basically has a p-i-n structure. Thus, the CdTe photocurrent effect corresponds to a region farther to the right in Fig. 4. The larger doping densities, and hence small depletion widths, typical of GaAs predict smaller photocurrent variations. Crystalline GaAs will also have a larger diffusion length and slightly larger voltage relative to V_{bi} than the polycrystalline cells, but these

two effects roughly compensate each other in terms of photocurrent-voltage dependence. For crystalline Si cells, the variations in photocurrent with voltage can be ignored, because the large minority-carrier diffusion length and small absorption coefficient correspond to the region at the lower left of Fig. 4.

Experimentally, Fardig and Phillips [6,7] have successfully used two techniques to determine J(V) in reverse bias. These are (1) the analysis of the voltage dependence of spectral response, and (2) the separation of linear and non-linear J vs. V components. Their work on CdTe cells predicts ΔJ_L magnitudes similar to those deduced above. However, both these techniques experience increasing uncertainties in forward bias and may not easily extrapolate to give reliable values of ΔJ_L at operating voltages.

Capacitance Analysis

Analysis of capacitance data from $CuInSe_2$ and $Cu(In,Ga)Se_2$ cells has gotten considerably cleaner in recent years as the overall quality of the cells has improved. It has become rare to see frequency dispersion due to large numbers of trapping states. We can with much more reliability use capacitance vs. voltage data to map out the spatial distribution of carrier density in the absorber, which often correlates with gradients or steps in the fabrication process. At the same time, it has become clear that 1 MHz is generally too high a frequency for capacitance measurements that are amenable to reliable interpretation. Since one must always assume a certain amount of leakage with polycrystalline diodes, one is essentially forced to assume parallel addition of real and imaginary conductuctance contributions [8]. Indeed, as seen in Fig. 5, the measured capacitance is quite independent of frequency over a substantial range. At frequencies above 400 kHz in this case the external circuit inductance produces a rapid, but artificial, rise in the measured capacitance. In other cells with higher series resistance, there is a precipitous drop in measured capacitance as one approaches 1 MHz. Some compensation for the inductance and resistance of the leads is possible, but in general the measurement uncertainty will increase with the amount of compensation required.

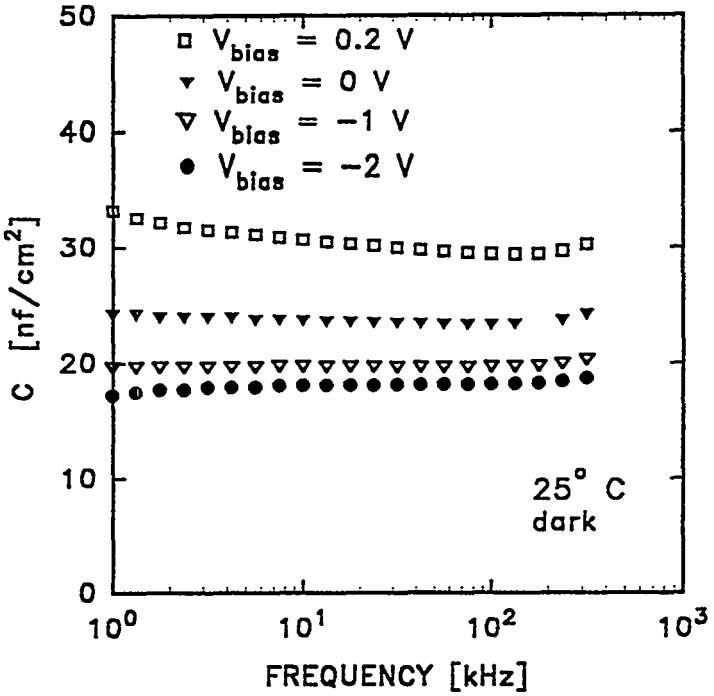

Figure 5. Capacitance vs. frequency for NREL Cu(In,Ga)Se_2 cell M1174-14#3 assuming parallel mode.

Fig. 6 shows the C^{-2} vs. V plot for the same cell. A measurement frequency of 300 kHz was chosen, but the data is initially identical for all frequencies between 3 and 300 kHz as implied by Fig. 5. Shown at the right of Fig. 6 is the depletion width corresponding to the capacitance values. The voltage intercept is plausible in this plot, suggesting no major change in hole density as one approaches the interface. There is a distinct change of slope near -1V, or a depletion width of 0.5 μm. The flatter slope means a larger hole density for distances farther than 0.5 μm from the junction.

Figure 7 quantifies the hole density as a function of distance from the junction. It uses exactly the same capacitance data as was used to construct the previous figure, and it displays the features of the hole density profile that were implied by Fig. 6. Specifically, it shows no sign of a low carrier concentration dead-layer near the interface, and it shows transition between Cu(In,Ga)Se_2 layers 0.5 μm from the interface.

In contrast, Fig. 8 shows the C^{-2} vs. V data and the deduced hole density profile for NREL's highest efficiency $CuInSe_2$ cell. In this case, there is a very uniform hole density in the bulk

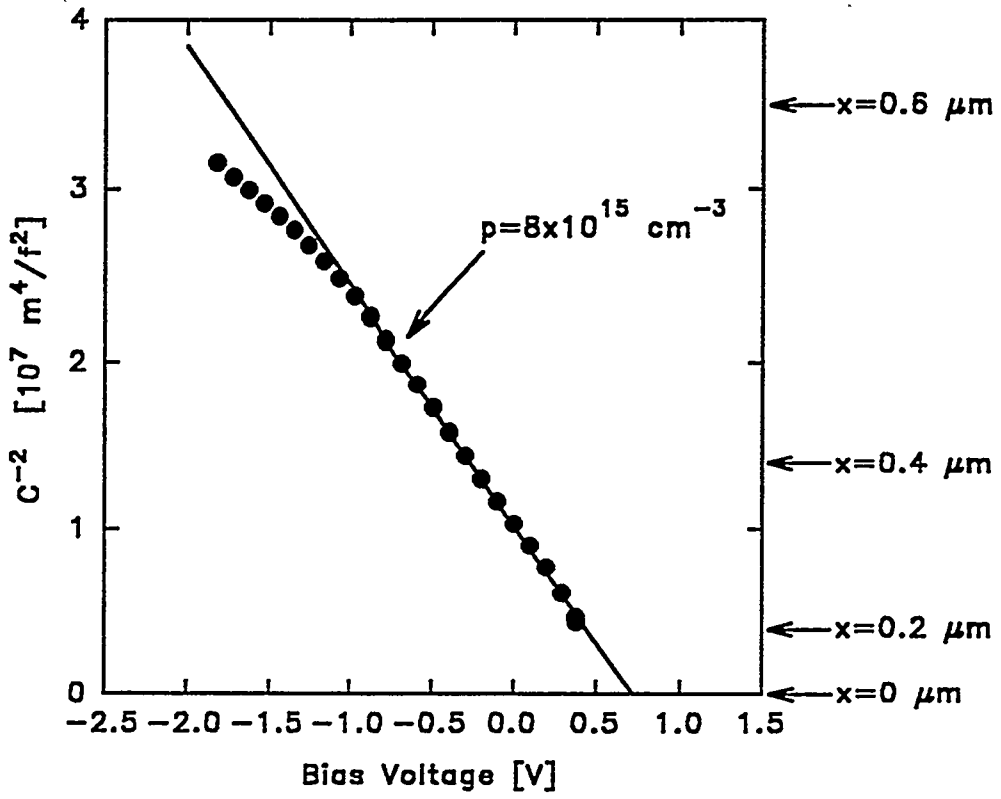

Figure 6. Bias dependence of C^{-2} for NREL cell M1174-14#3.

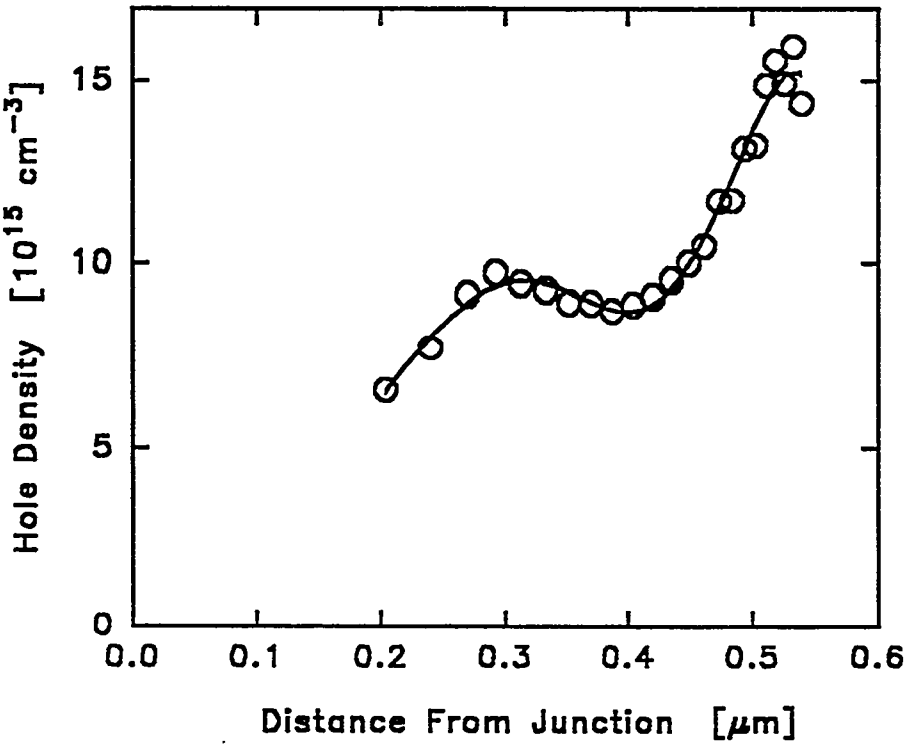

Figure 7. Spatial profile of hole density deduced from capacitance data for cell M1174-14#3.

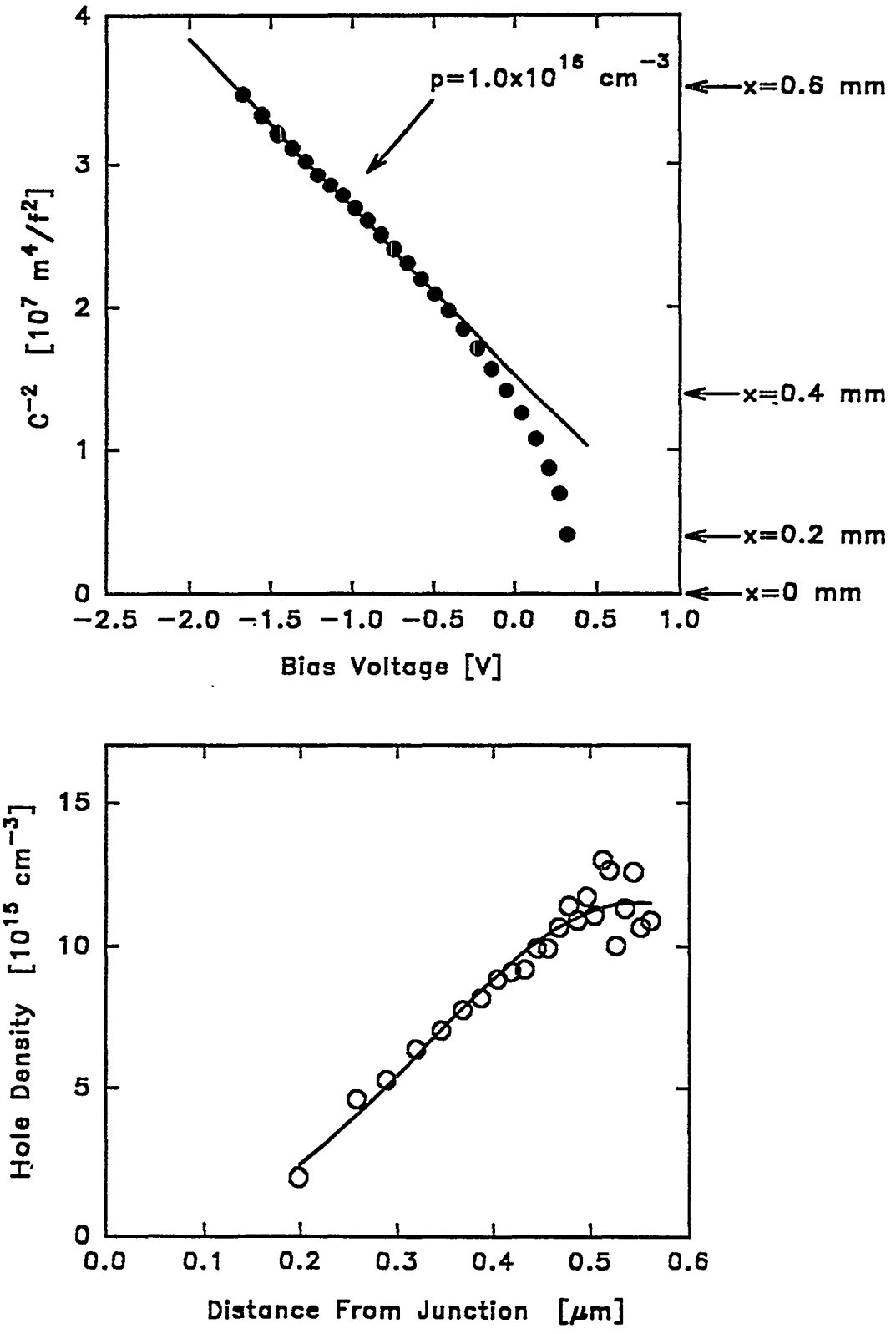

Figure 8. Bias dependence of C^{-2}(top) and corresponding spatial profile of hole density for NREL $CuInSe_2$ cell M1201-14#4.

part of the absorber. Within approximately 0.3 μm of the interface, however, the carrier density drops sharply, probably because of greater compensation due to an increased density of donor states in this region. Note that the signature in the C^{-2} vs. V plot for such a junction layer are an artificially large intercept of the extrapolated reverse bias data and a negative curvature in forward bias.

Capacitance data for CdTe cells is not yet as clean as that discussed above. The frequency range for reliable interpretation is narrower and many cells display effects due to extraneous trapping states. Fig. 9 summarizes the capacitance information typical of CdTe cells. Note that the C^{-2} scale is a factor of 25 larger than that used in Figs. 6 and 8. The topmost curve shown was quite common up until a few years ago. The capacitance is essentially independent

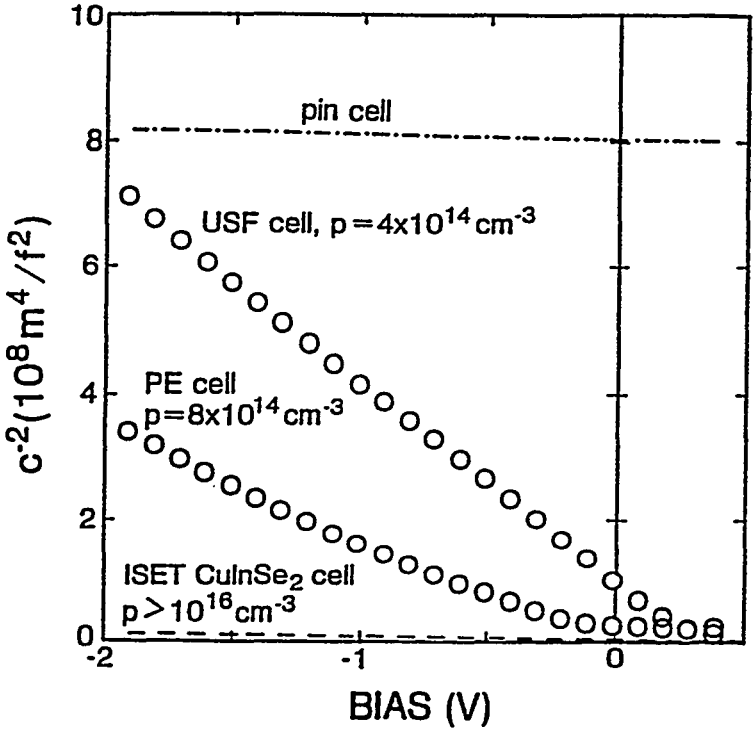

Figure 9. Comparison of p-n and p-i-n CdTe cell capacitances, plus that typical of $CuInSe_2$.

of voltage and corresponds to the physical thickness of the CdTe layer, about 2½ μm in this case. Since the CdTe carrier density is too small to be measured by this technique, it has been referred to as an intrinsic or i-layer cell. More recent CdTe cells of South Florida have C^{-2} vs. V curves with a more standard appearance, but slopes that correspond to very low carrier

densities. Differences in cell operation between the "i" cells and the "p" cells are much less pronounced than the dramatic difference in capacitance, and one should probably not make a qualitative distinction. For reference a typical $CuInSe_2$ curve is included on Fig. 9, but its features cannot be seen on this scale.

Annealing Effects

The need for post-deposition thermal annealing of some types $CuInSe_2$ and CdTe solar cells has been recognized for some time. Less recognized is which loss mechanisms are reduced by the annealing process and what are the specific consequences of over-annealing. Building on an earlier study [9], individual $CuInSe_2$ cell parameters were tracked as a function of annealing temperature [10]. The cells used were fabricated by vacuum evaporation at the Institute for Energy Conversion (IEC) at the University of Delaware.

Fig. 10 shows typical current-voltage curves following anneals of several temperatures. The cells improved after they were heated at temperatures up to 275°C, after which the cells began

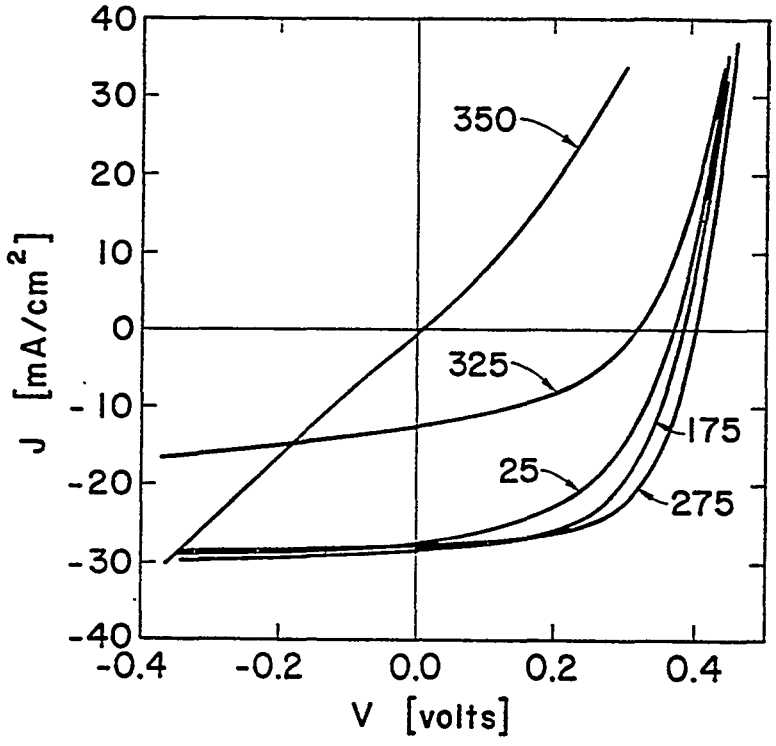

Figure 10. Current-voltage curves for IEC cell 3190113-12 following anneals at the temperatures indicated.

to degrade rapidly, becoming nearly ohmic and insensitive to light at 350°C. This degradation has been noted previously. It is caused by a combination of higher series resistance, lower shunt resistance, larger forward recombination current, and a lower photogenerated current.

The top part of Fig. 11 shows room temperatures values of J_{SC} and V_{OC} as a function of annealing temperatures (T_A). Changes in J_{SC} were not a strong function of spectral content. The curves roughly track each other. They both rise slowly at low T_A and decline rapidly for high T_A. However, J_{SC} begins its decline at 250°C, whereas V_{OC} starts to drop at 300°C. Note that the maximum value of J_{SC} occurs at 225°C which is generally cited as the optimum anneal temperature for vacuum evaporated $CuInSe_2$ [11]. The implication of different onset temperatures for the decrease in V_{OC} and J_{SC} is that more than one physical mechanism is present.

To help separate the degradation mechanisms, the annealing effects on the diode quality factor A and series resistance R_S are examined separately, as shown in the lower part of Fig. 11. There is a positive correlation between the value of A and the amount of forward recombination current. The forward current opposes the photogenerated current, and any increase results in lower operating voltages. In Fig. 11, the diode quality factor decreases between 175°C to 275°C, exactly the same region that V_{OC} increases. The increase in V_{OC} is due to lower recombination, and most likely corresponds, on the microscopic level, to oxygen passivation of grain boundary defects. The series resistance closely follows the trend of A. The decrease in the series resistance is due to an increase in mobility which follows from the decrease in defects. As the temperature is increased past 300°C, the mobility falls rapidly resulting in a large series resistance increase.

The top of Fig. 12 shows the intrinsic layer thickness d_i as a function of the cells annealing temperature. Note that a measurable intrinsic layer first develops at 275°C and grows rapidly at higher temperatures. The intrinsic thickness at 350°C is about 1.5 μm which is half the thickness of the $CuInSe_2$ layer.

The hole density increases steadily with annealing temperature, as shown in the middle part of Fig. 12. This increase of p corroborates the thesis that compensating donor states are eliminated

through oxidation at the lower annealing temperatures. As the temperature is increased beyond 275°C and S and Se diffuse across the junction, one might expect the hole density to decrease. This decrease, however, is not apparent in the capacitance data, since as the intrinsic layer

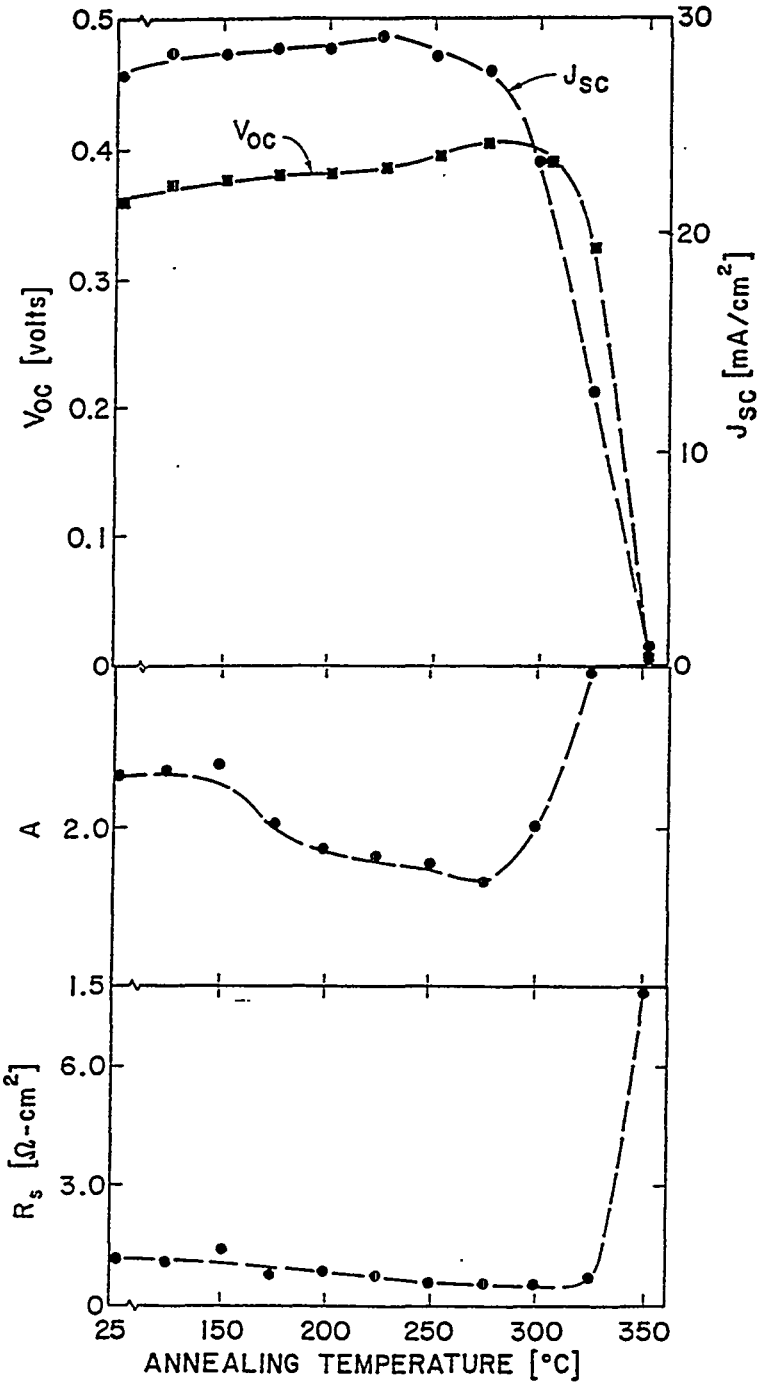

Figure 11. Variation of J_{SC}, V_{OC}, A, and Rs with annealing temperature, IEC cell 3190113-12.

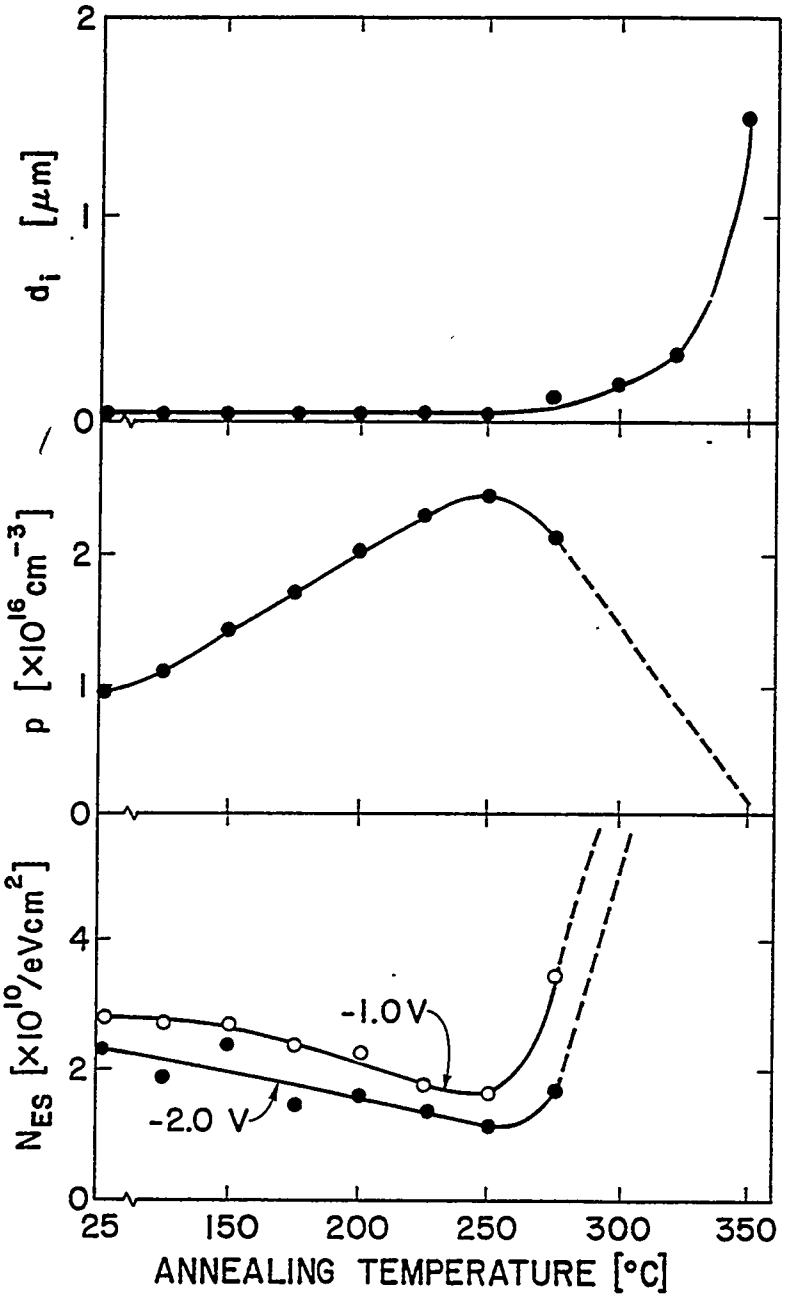

Figure 12. Intrinsic layer thickness d_i, hole density p, and extraneous state density N_{ES} deduced from capacitance date for IEC cell 3190113-12.

develops, the depletion region is moved deeper into the $CuInSe_2$. Thus, a different physical region is probed. The dashed line represents the anticipated result if the same physical region were measured.

The number of extraneous states N_{ES} in the depletion region is proportional to the difference in capacitance measured at high and low frequencies [8]. N_{ES} decreases with annealing temperature

until reaching a minimum at 250°C. This corresponds to the reduction of compensating donor defects discussed above. Note that care must be used in interpreting N_{ES} at temperatures above 275°C, because of the development of the intrinsic layer. The dashed line is the expected result in the absence of an intrinsic layer.

Annealing effects on other evaporated and selenized $CuInSe_2$ cells have been studied less extensively. The general degradation patterns shown above are always present, but the onset of degradation can occur at significantly lower temperatures.

TIME-DEPENDENT VOLTAGE

An increase in voltage with time following the onset of illumination or a switch to forward bias has been observed in almost all $CuInSe_2$, $Cu(In,Ga)Se_2$ and CdTe cells. An example of such an increase is shown in Fig. 13. Note that it takes place over at least 7 decades of time. The difference in V_{oc} measured at different times is about 20 mV, or 4% of its value.

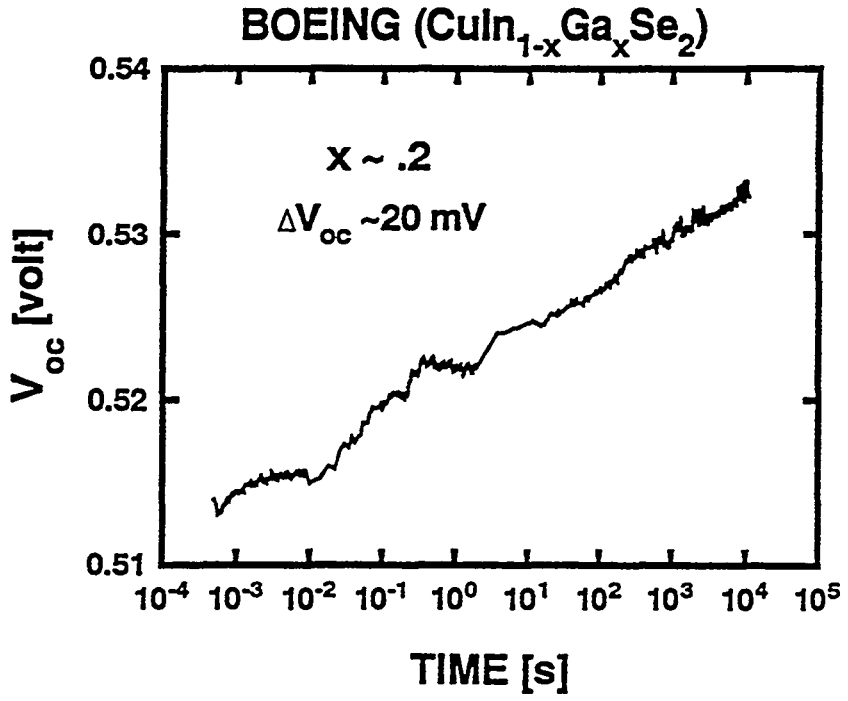

Figure 13. Transient voltage following switch to open-circuit conditions.

The effect of the time-dependent voltage on the full current-voltage curve for a typical $CuInSe_2$ cell is shown in Fig. 14. The curve labeled "forward sweep" was taken as quickly as possible after the cell had been held at zero bias for over an hour. The other curves were also taken quickly, but after the cell had been held at V_{oc} for the times indicated. Obviously different curves will be recorded depending on the speed and other details of the measurement process. In particular, one would clearly expect different results from a pulse-simulator measurement than those acquired with the sun or other quasi-dc sources of illumination.

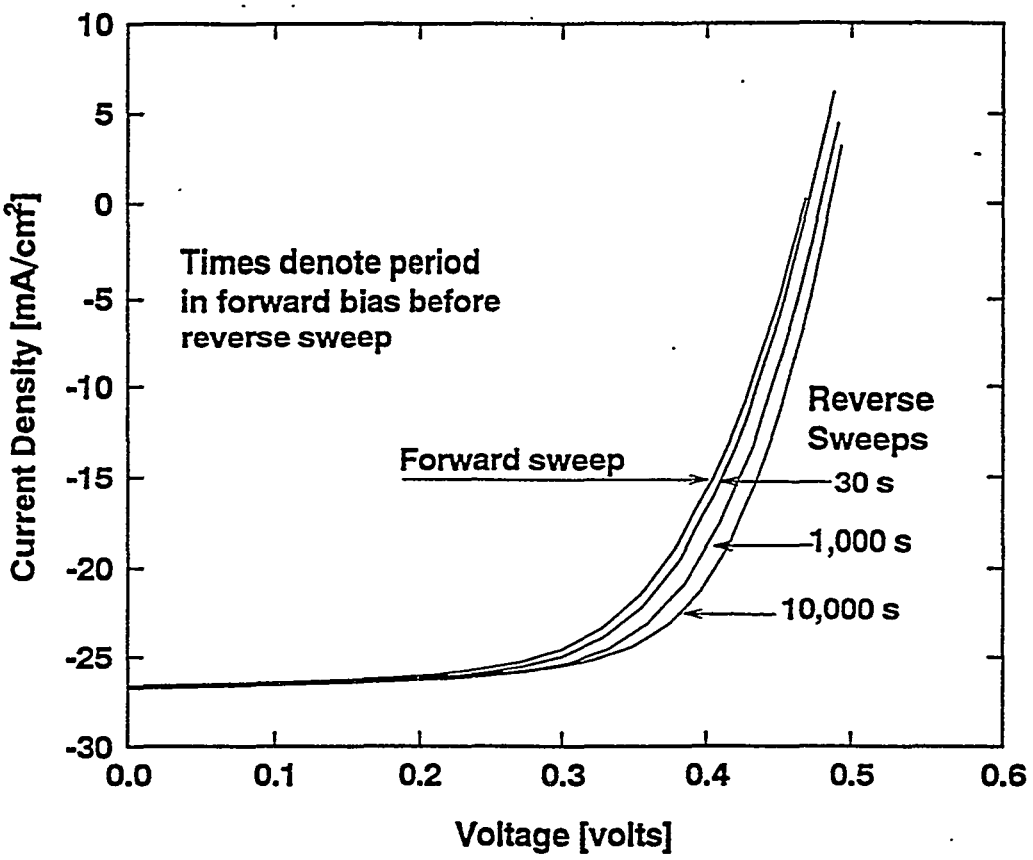

Figure 14. Variation in J-V curve with initial conditions.

The apparatus used to study the time-dependent voltage of individual cells is shown in Fig. 15 and has been described in more detail elsewhere [12-14]. Voltage is recorded as a function of time using a digitizing scope for the 0.5 ms to 2 s range and a digital volt meter for longer times. The onset of illumination or forward bias is controlled by one of four modes, each of which can be done in less than 1 ms:

(1) Switch from short to open circuit under constant illumination.

(2) Switch from zero (short circuit) to finite (operating condition) load resistance under constant illumination.

(3) Switch from dark to light using a camera shutter.

(4) Switch from zero to finite constant current in either dark or light.

There are also variations such as switching from reverse bias to V_{oc} and from one light intensity to another.

The most difficult technical issue for the time-dependent measurements is good temperature control for the duration of the measurements. Temperature variation of 1°C corresponds to

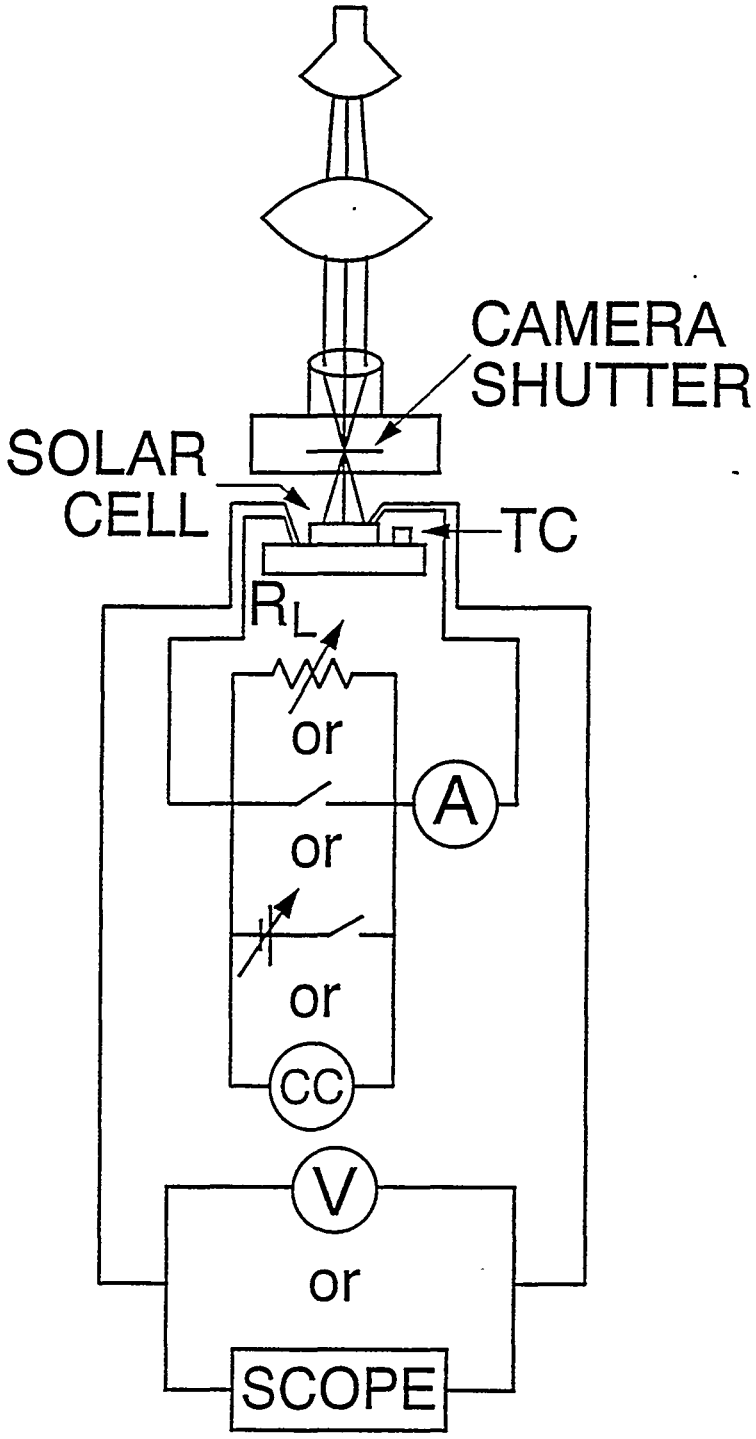

Figure 15. Schematic apparatus for time-dependent voltage measurement.

a voltage error of 2mV, which is the limit of the measurements at present. In all reported measurements, cool nitrogen gas is flowed over the cell surface and a feedback controlled IR heater is used for fine tuning. This arrangement also allows measurements to be repeated at different base temperatures.

Table 1 gives a summary of the magnitude of the voltage change observed in a variety of polycrystalline thin-film cells. Only the single-crystal silicon cell used for reference showed no measurable effect, although the highest efficiency $CuInSe_2$ cell fabricated at NREL displayed only a marginally observed increase in voltage. In general, it appears that the effect is diminished as junction quality is improved.

Table 1. Change in V_{oc} between 1 ms and 2000 s after the onset of illumination

Cell Type	Origin	V^{oc}(long t)	ΔV_{oc}[mV]
Silicon		512 mV	0±2mV
$CuInSe_2$	ISET	452	22
		460	18
	IEC	440	15
	NREL		
	Standard process	432	17
	Variable fluxes	424	15
	Highest efficiency	485	2
	Siemens		
	Standard	446	4
	no CdS	487	6
$CuInSe_2$+ (high E_g)	Boeing	533	27
	NREL	652	4
	Siemens	619	20
CdTe	Photon Energy	764	38
	U South Florida	858	36

An obvious question about the voltage-increase effect is whether it is driven by illumination or bias. The evidence points strongly to the bias history. Fig. 16 compares the "switch" measurement (short to open circuit under constant illumination) with the "shutter" measurement (dark to light). The "shutter" measurement requires a small correction since the temperature

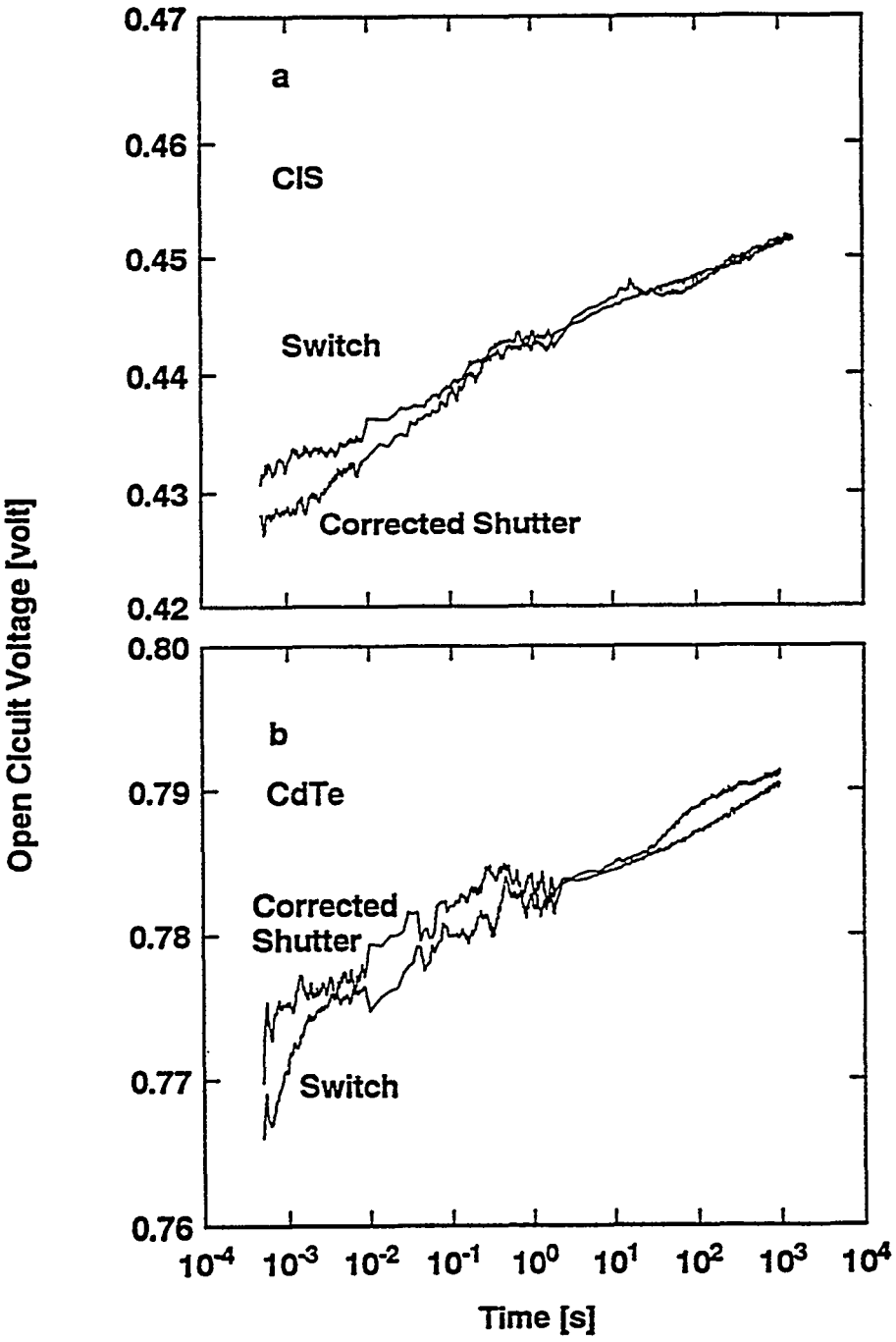

Figure 16. **Comparison of switch and shutter measurements for $CuInSe_2$ and CdTe cells.**

gradient across the substrate changes between dark and light. The fact that the gradient is in the opposite direction for the CdTe superstrate geometry is convenient in determining its magnitude.

Further evidence that the transient voltage effect is due to the voltage history is found in Fig. 17, which shows curves for an ISET selenized $CuInSe_2$ cell and an IEC evaporated cell that were both held at a bias near V_{oc} in the dark for over an hour before the measurement.

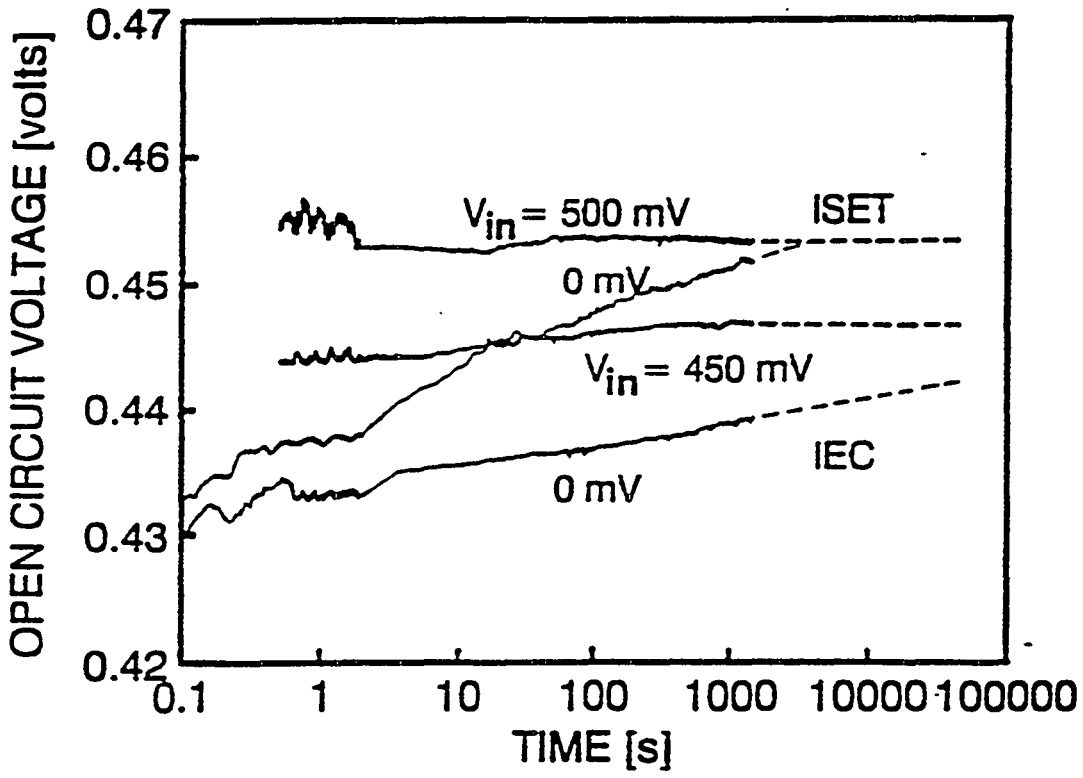

Figure 17. Comparison of zero and near-V_{oc} pre-bias for $CuInSe_2$ held in dark prior to measurement.

V_{in} is used to indicate the value of this initial bias or pre-bias. The light was turned on, the circuit quickly opened (< 1 s), and the voltage monitored as a function of time. The ISET cell was held at V_{in} + 500 mV prior to the measurement so that the voltage actually decreases slightly before equilibrating. In both cases the transient voltage effect after illumination was quite small. Also shown in Fig. 17 are curves when the cells were shorted prior to the measurement. (V_{in} = 0) These curves show the full transient voltage effect. The contrast argues strongly that the effect is indeed driven by the voltage history.

Still further evidence that the transient voltage is independent of light is seen by comparing a dark constant-current corresponding to a voltage near V_{oc} with a V_{oc} versus time measurement. This was done with the Boeing $Cu(In,Ga)Se_2$ cell used for the initial example in Fig. 13. The result is shown in Fig. 18. The only difference outside of the noise level is a slight translation in voltage due to the dark-current value chosen. The strong evidence is that the effect is caused by the voltage history of the sample and by not the illumination.

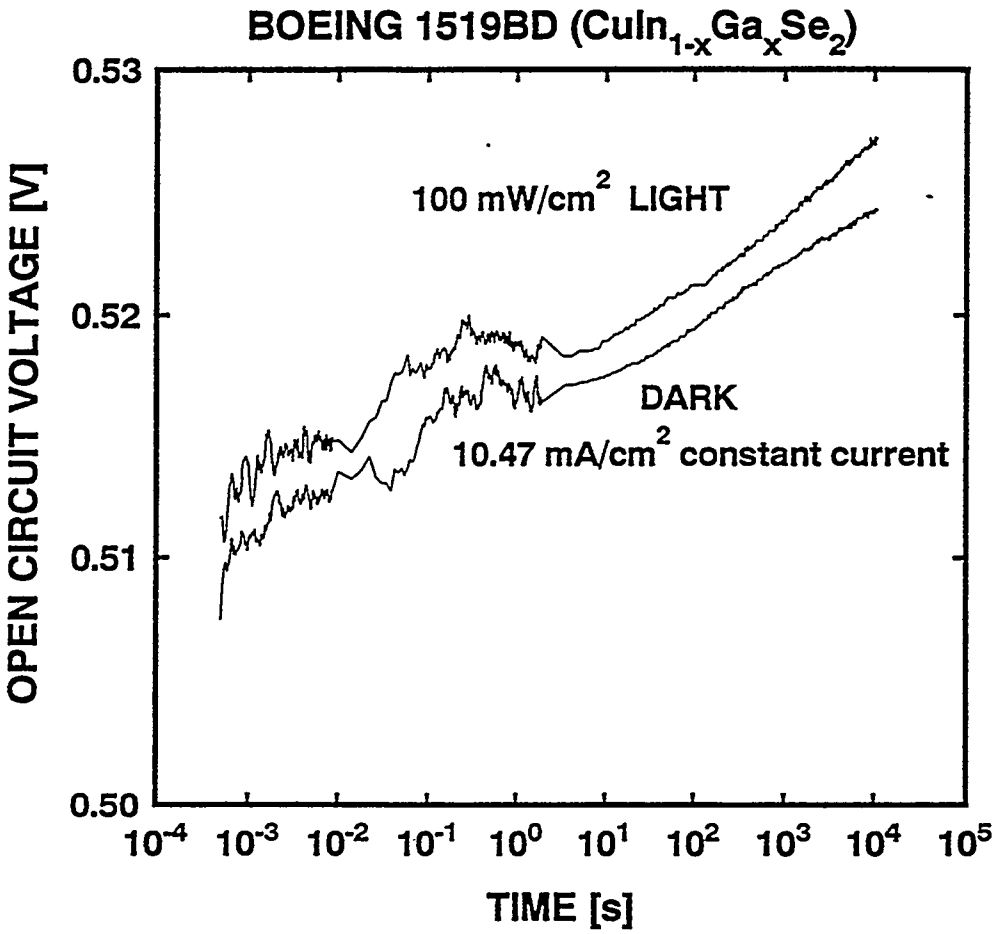

Figure 18. Comparison of V_{oc} increase to that of voltage produced by constant dark current.

A time-dependent voltage that is related to the bias history of a diode is highly suggestive of a mechanism involving long-lived trapping states that depopulate under forward bias. The time constants of such traps would correspond to several decades of time over which voltage changes are observed. Ref. 14 makes a strong case that these trapping states are in the upper half of the absorber bandgap and increase in density as one approaches the junction. Depopulation of these states would modify the bandshape in the depletion region, resulting in reduced forward current,

or equivalently higher voltage if current is held constant [14]. It seems entirely plausible that the number of such states will decrease as improved cell-fabrication techniques produce material that is electronically more similar to single crystals.

The repopulation of trapping states when voltage is returned to zero should take place with approximately the same time constants as the depopulation process. Fig. 19 confirms this

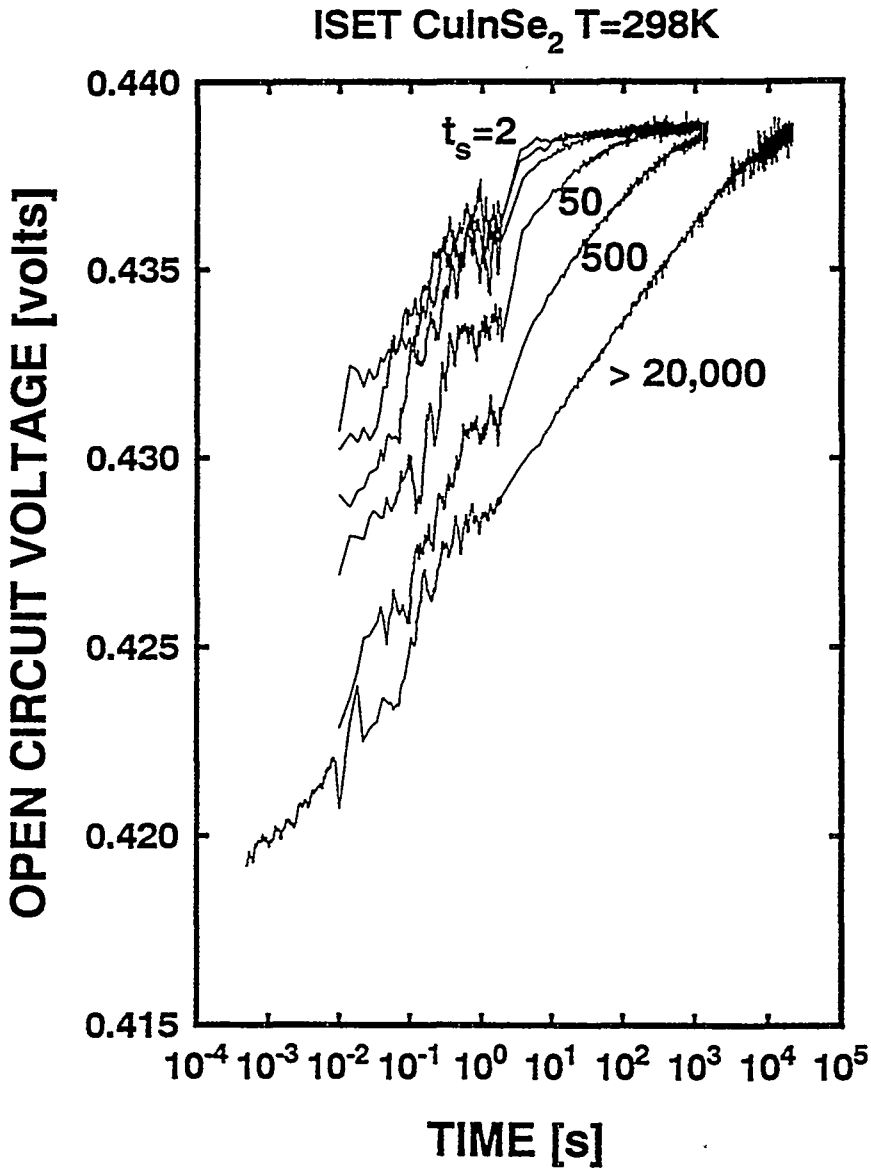

Figure 19. Relaxation behavior of selenized ISET cell under constant illumination. τ_s is the time the cell was shorted.

point by showing the effect of returning the cell to zero bias for periods of 2, 5, 10, 50, 500, and over 20,000 s following a long time at V_{oc}. During the shorter periods of time, only a

fraction of the traps repopulate, and one can see that the time required to restore the long-term value of V_{oc} is approximately the same as the time allowed for repopulation.

Fig. 20 examines the voltage increase following a shift between specific finite voltages. It is an attempt to define the voltage range primarily responsible for the changes in population

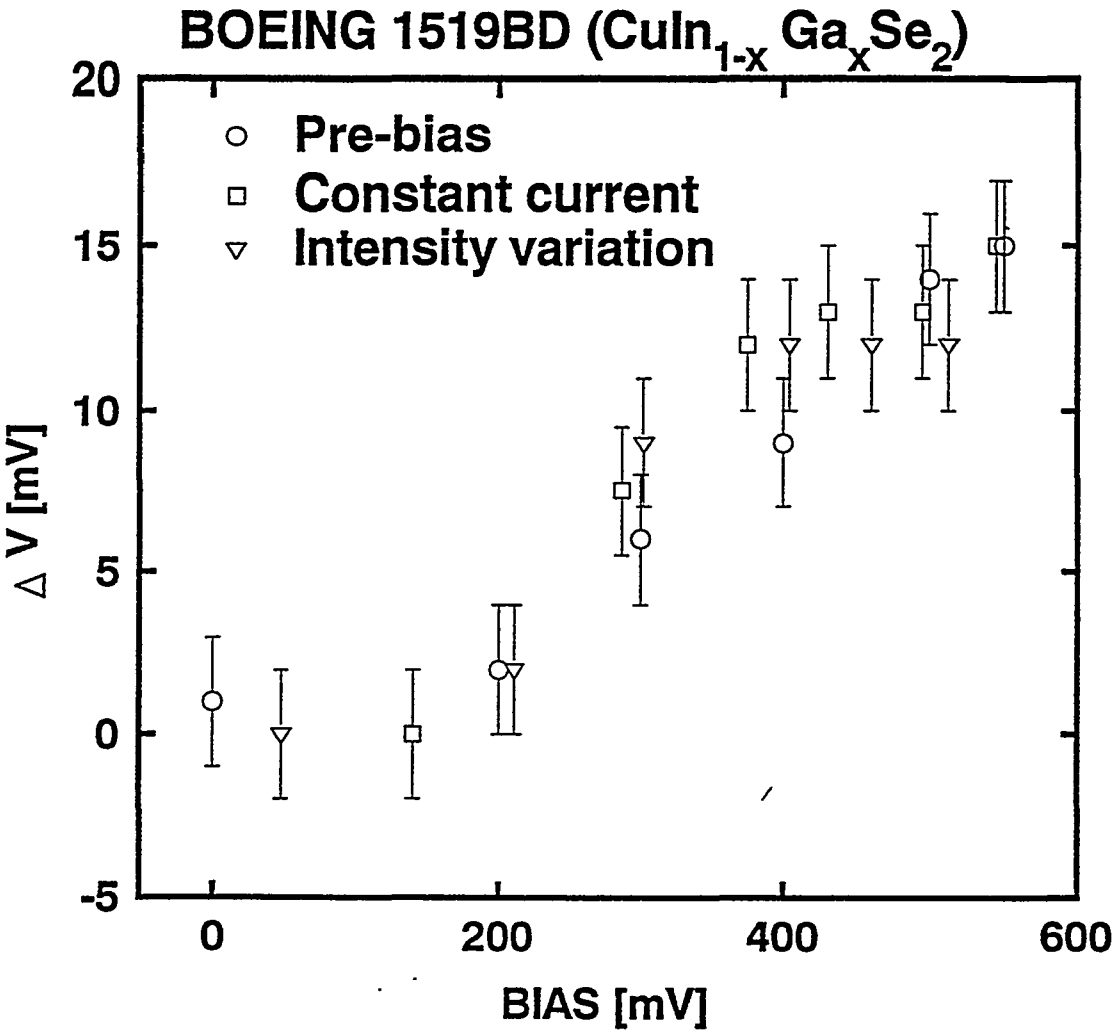

Fig. 20. Magnitude of voltage change after bias is switched using three separate techniques.

of the long-lived trapping states. Data taken by three different techniques is included in Fig. 20: (1) A shift from a range of pre-biases to V_{oc} just before the onset of illumination. (2) A switch from zero to a positive constant current in the dark. (3) A change from dark to a range of illuminations between 0.1 and 100 mW/cm^2. All three techniques gave the same shift relative to the zero-bias reference. The proposed interpretation is that most of the depopulation of long-

lived traps takes place in the voltage range between 200 and 400 mV. Other cells show a similar pattern. For CdTe cells, however, the depopulation takes place at somewhat larger voltages.

There are some variations in time-dependent voltage with temperature. Fig. 21 shows the voltage increase at four different temperatures for a selenized $CuInSe_2$ cell fabricated at ISET.

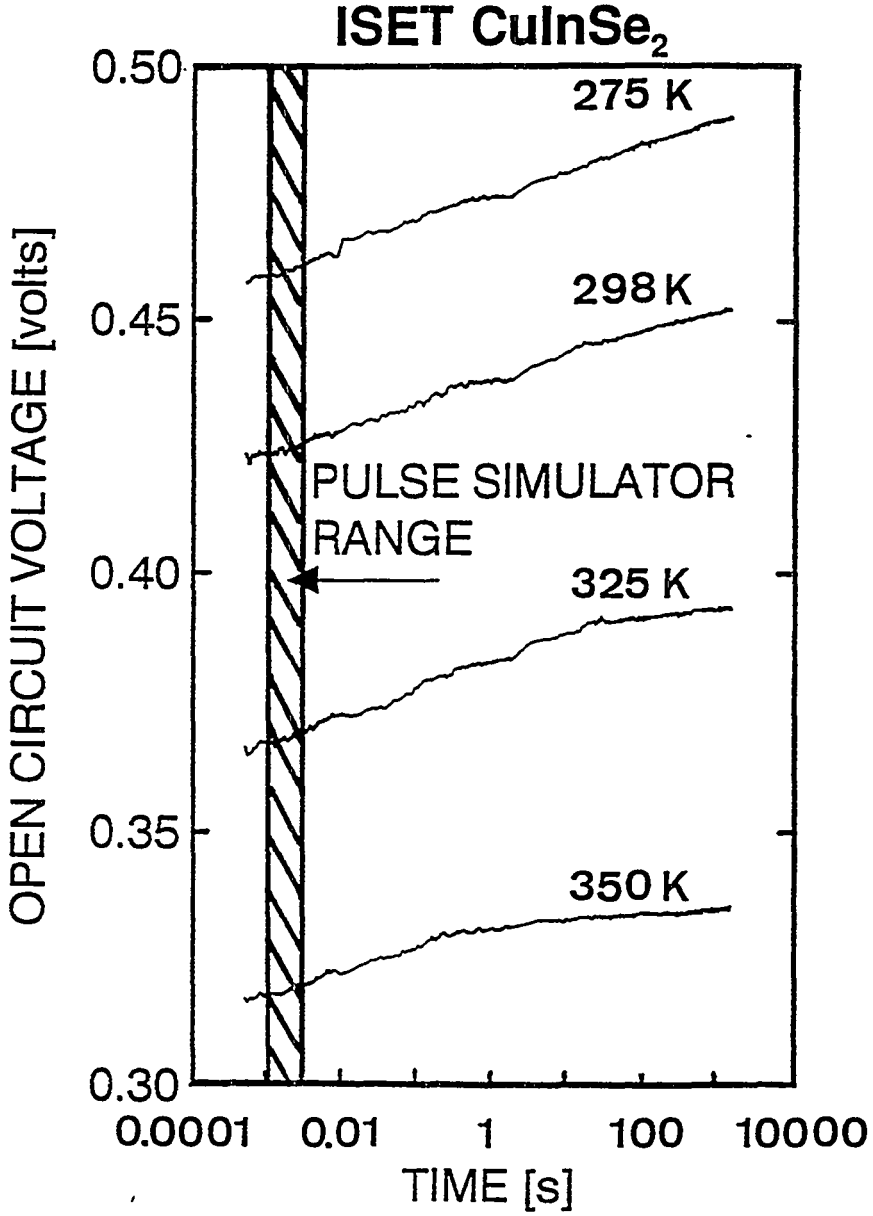

Figure 21. **V_{oc} transients for a typical selenized $CuInSe_2$ cell at four temperatures.**

Only at the highest temperature does the voltage clearly saturate. It is likely that the time constants become longer at lower temperatures and that the states responsible for the low-

temperature effect are too fast to be observed at the higher temperatures (off the graph to the left). A practical consequence of the lack of low-temperature saturation in a practical time span is that dV_{oc}/dT will be artificially low, and hence low-temperature values of V_{oc} on a V_{oc} vs T plot will fall below the higher temperature extrapolation.

In summary, the time-dependent voltage has both physical and practical implications for thin-film polycrystalline solar cells. Table 2 lists the primary features and conclusions:

Table 2. Primary features of the time-dependent voltage effect

1.	Voltage of most thin-film polycrystalline cells continues to increase after a shift to forward bias.
2.	The increase is dependent on voltage history, not illumination history.
3.	The likely explanation is depopulation of long-lived traps, which modifies the band shape in the depletion region.
4.	The traps have time constants spanning at least the 1 ms to 10 ks range. Energies are just above mid-gap, and densities are comparable to absorber carrier densities.
5.	Relaxation takes place with essentially the same range of time constants.

SPECIFIC RESULTS

CdTe Cells

A comparative analysis of CdTe cells from several different laboratories and several different fabrication techniques was prepared in early 1992 [5]. Table 3 lists the cells examined. In general these are the highest efficiency cells from each laboratory at that time.

Table 4 gives the individual parameters deduced for each cell. For reference, the parameters required for a hypothetical 18% cell are given in the left-hand column. Many of the existing cells approach, or even exceed, the target parameters in some areas, but fall short in others. If one were allowed to pick the best individual parameters from Table 4, one could construct a 17.8% CdTe cell.

Since Tables 3 and 4 were generated, most of the improvements in high-efficiency CdTe cells have taken place at the University of South Florida (USF). Fig. 22 shows the J-V curves for three USF cells: (1) The 14.6% cell included in Tables 3 and 4 [15], (2) a 15.0% cell which has the best junction features, and (3) a 15.8% cell which has the highest CdTe efficiency to date [16]. Also shown is the 18% target defined in Table 4. Although the 15% cell has the smallest photocurrent, one can see that it has the sharpest experimental knee. It also has the largest V_{oc}, although the differences between the experimental cells are too small to see on the graph.

The room temperature forward current for the three CdTe cells under illumination is shown in Fig. 23. Also shown with a solid line is the forward current for the 18% target cell, and with solid circles the dark data for the 15% cell. The dashed lines are fits with the series and shunt resistance effects removed ($R_S \rightarrow 0$, $R_{sh} \rightarrow \infty$). The fit for the 15% cell is closest to the target curve. At any selected voltage, its forward current under illumination is smaller than that of the other two CdTe cells. Its dark forward current is in fact less than the target curve. The difference between light and dark fits ($\sim$30 mV) is smaller than that seen in earlier cells, but

Table 3. Early 1992 summary of High-Efficiency CdTe Solar Cells

Manufacturer	CdTe Deposition	Highest Efficiency	Cell No.	Source of Data
University of South Florida (USF)	Close Space Sublimation	14.6%	11-4-8A	Our measurement NREL measurement Published
British Petroleum (BP)	Electrodeposition	14.2%		Published
Photon Energy (PE)	Spray Process	12.7%	3 151 A1	NREL measurement Our measurement
Microchemistry, Ltd. (MC)	Atomic Layer Epitaxy	11.5%*		Published
Matsushita (MT)	Screen Printing	11.3%		Published
University of Queensland (QL)	Electrodeposition	11.2%*		Published
Batelle Europe (BE)	Close Space Sublimation	11.0%		Published
Institute of Energy Conversion (IEC)	Physical Vapor Deposition	11.0%	40723.11-2	NREL measurement
Georgia Institute of Technology (GIT)	Metal-Organic Chemical Vapor deposition	10.9%	D3	Our measurement NREL measurement Published

* Current density adjusted to NREL measurement and/or quantum efficiency consistency

Table 4. Comparison CdTe of Cell Parameters (100 mW/cm^2 global; 25°C)

	18% Target	USF	BP	PE	MC	MT	QL	BE	IEC	GIT
Photocurrent [Ma/CM^2]	26	24.4	23.5	26.2	19.5	21.1	24.0	22.8	20.1	22.1
Photon Losses [Ma/cm^2]										
Reflection	2	1.5		2	2			2	2.5	2
Window Bandgap	1.5	1		1	8			3	5.5	5.5
Deep Penetration	1	1		1.5	1			1	1.5	1
Unidentified	0	3		0	0			1.5	1	0
Open Circuit Voltage [Mv]	875	850	819	790	810	797	720	750	789	745
Maximum-Power Voltage [Mv]	750	686	690	585	655	634	550	599	625	588
Fill Factor [%]	79	70.5	74	61.5	73	67	65	65	69	66
Diode Quality Factor	2.0	2.6	1.9	3.6	2.2	3.0	2.7	2.8	2.75	2.8
Series Resistance [Ω-cm^2]	0	0.5	0.3	0.7	0.3	0.5	0.5	0.7	0.35	0.3
Shunt Resistance [Ω-cm^2]	∞	2000	1000	600	2400	1500	700	800	1700	800
Efficiency [%]	18	14.6	14.2	12.7	11.5	11.3	11.2	11.0	11.0	10.9

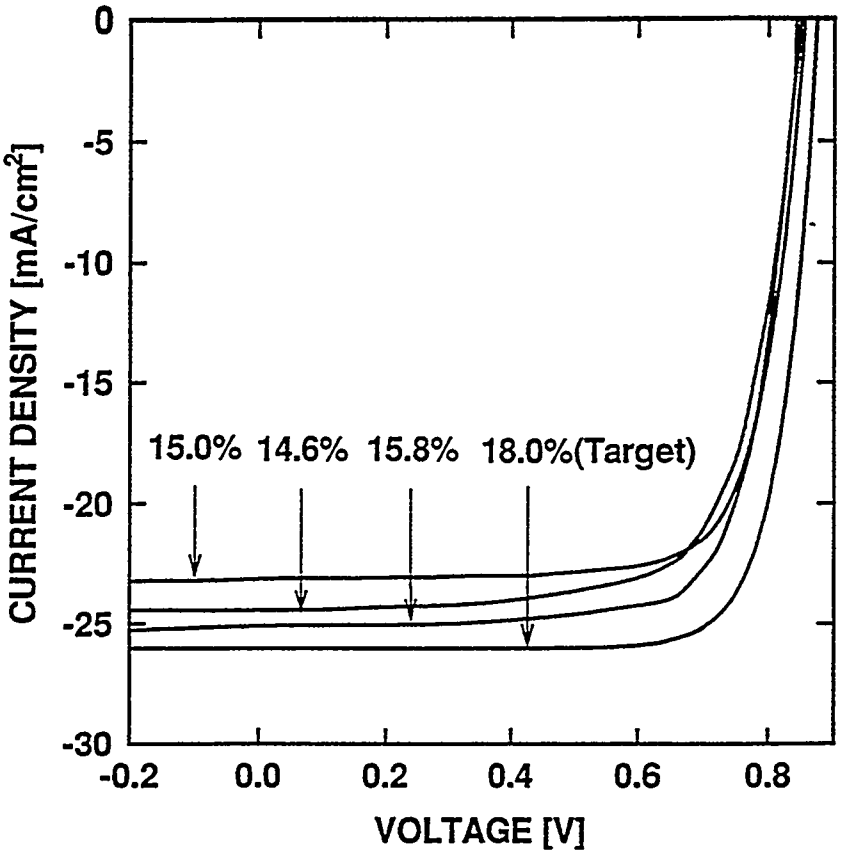

Figure 22. Current-voltage curves for highest-efficiency 1991 USF cell (11-4-8A, 14.6%) highest-efficiency 1992 cell (6-1B-6B), 15.8%), best-junction cell (5-1A-12B, 15.0%), and target cell (18%).

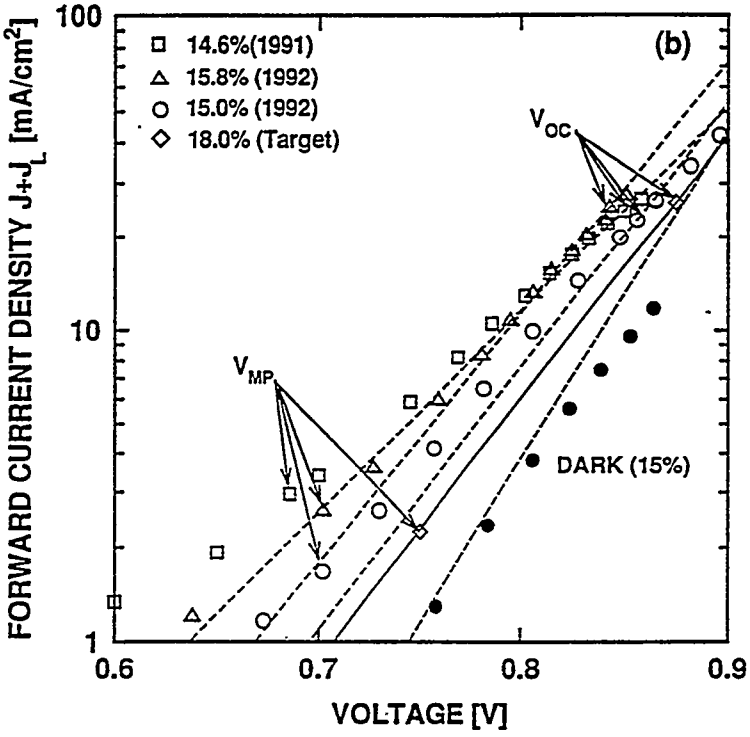

Figure 23. Comparison of forward diode currents for same CdTe cells.

does imply some modification of barrier shape by illumination. In any case, the junction barrier of the 15% cell is significantly improved in comparison with the best cell from one year earlier, and even in comparison with the highest efficiency cell.

Quantum efficiency measurements were used to quantitatively separate the individual photocurrent loss mechanisms [17]. Fig. 24 shows the lost photon fraction, one minus the measured quantum efficiency, as a function of wavelength for the three USF cells under discussion, as well as the highest-current Photon Energy CdTe cell [5]. The individual losses (which are given for a number of other cells in Table 4) are calculated by attributing a loss mechanism to each lost-photon region, multiplying by an appropriate solar spectrum [3] in in current units, and integrating over wavelength. Window absorption (the loss at short wavelengths due to absorption in the window layer of the cell) for the 15% cell is high (4 mA/cm^2) compared to the highest efficiency USF cell (2½ mA/cm^2) and the earlier USF cell (1 mA/cm^2). In the 1992 cells all photon losses are accounted for by the window absorption, reflection (nearly wavelength independent), and deep penetration (at long wavelengths). The 1991 cell, however, had an unexplained mid-wavelength loss of 2½ ma/cm^2. If the photocurrent losses of the best-junction USF cell were equal to those of the highest efficiency cell at that time, its efficiency would be 16.3%. If they equalled the highest-current Photon Energy cell, the efficiency would be 17%.

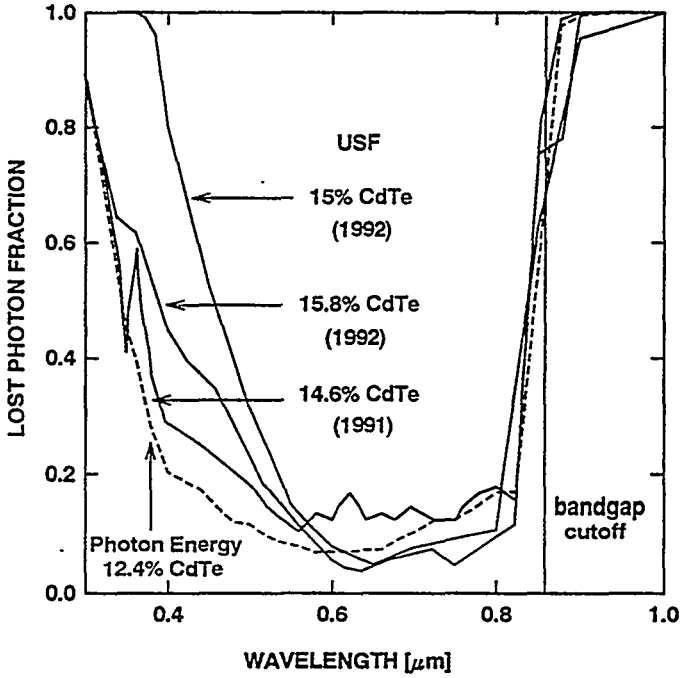

Figure 24. Comparison at photocurrent losses in three USF cells and the highest-current Photon Energy CdTe cell (12.4%).

Cell performance over time was measured for several 1992 cells and compared to the 1991 cell used above for reference (see Fig. 25). Initial and final measurements were done by NREL, intermediate ones at Colorado State. No changes in photocurrent or open-circuit voltage were observed either year. Also the A-factors and shunt resistances were flat over time within

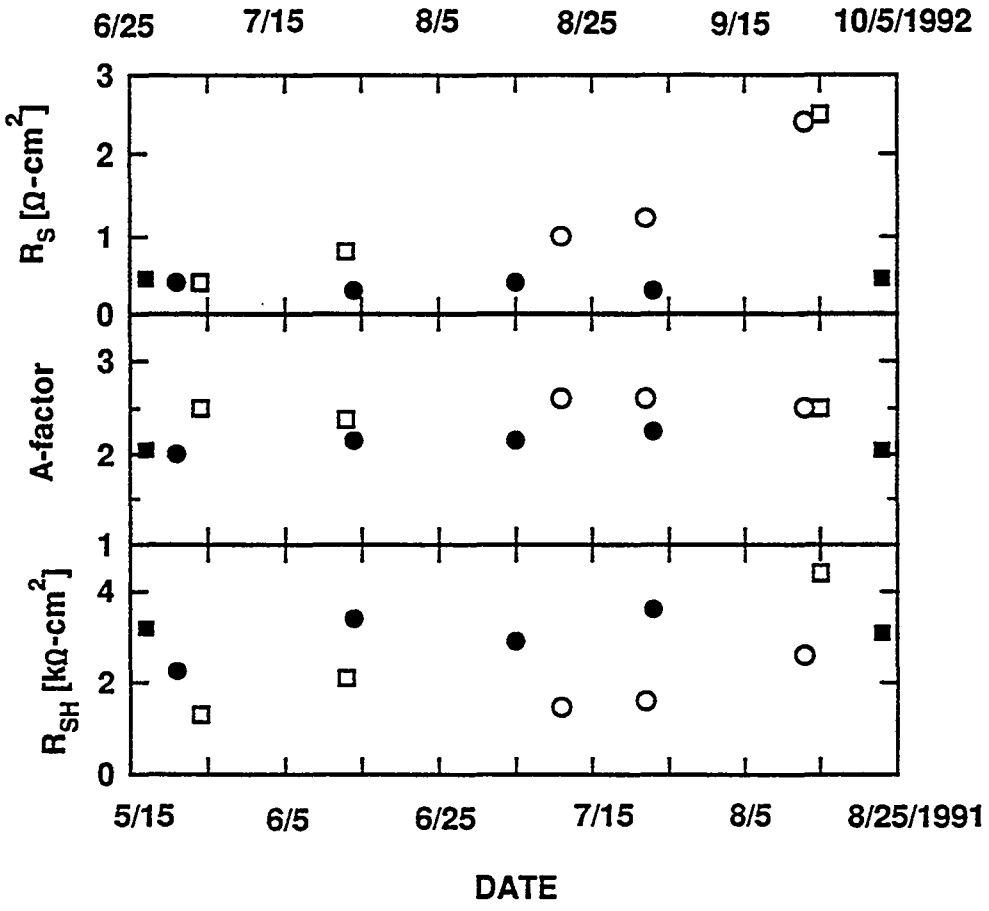

Univ. S. Florida CdTe Cell (100mW/cm^2, 25 °C)		
Year	1991	1992
Efficiency [%]	13.4-12.5	15
V_{OC} [mV]	840	860
J_{SC} [mA/cm^2]	22	23
fill factor	0.725-0.68	0.755
SERI/NREL	□	■
Colorado State	○	●

Figure 25. Fill factor parameters of 1991 and 1992 USF cells tracked for three months.

experimental error in both years. The series resistance of the 1991 cell, however, showed a gradual increase from 0.4 to 2.6 Ω-cm^2 over a three month period. This increase, possibly associated with contact degradation, resulted in a 40 mV decrease in V_{MP} and a corresponding fill-factor decrease from 0.725 to 0.68. In 1992, six cells were tracked,three kept in desiccant and three not. None of the parameters measured changed with time outside of experimental uncertainties. Thus, the series-resistance degradation has been effectively eliminated.

In summary, the efficiency improvements in recent USF-fabricated CdTe cells are primarily a result of success in keeping the forward recombination current well below that achieved by other groups. Not only is the dark forward current quite low, but the light-dark differential is relatively modest. The best-junction cells are in fact somewhat low in photocurrent, implying that efficiencies up to 17% should be fairly readily achievable. Furthermore, an earlier USF problem of series resistance degradation seems to have been solved, and the cells are now quite stable over at least a three-month interval.

$CuInSe_2$ Cells

The most significant recent progress with $CuInSe_2$ efficiency has been due to NREL [4] and the EUROCIS collaboration [18]. Figure 26 shows the room temperature current-voltage curves for the highest-efficiency cell from each group. For ease in comparison, the active-area current density was used. The NREL cell shown above is the same one used for example purposes in Figs. 3 and 8, and it appears in Table 1.

The EUROCIS $CuInSe_2$ cell has an excellent active-area current density (41mA/cm^2), due in large part to very good collection in the short wave length part of the spectrum. Presumably a relatively thin CdS window layer was used. The EUROCIS cell also has a very high open-circuit voltage (515mV). On the other hand, the NREL $CuInSe_2$ has three features related to its junction quality which we have not previously seen:

(1) The diode quality factor A is quite low ($\sim$1.2) and does not change measurably with temperature or intensity. This low value combined with very small series resistance R ($\sim$0.15 Ω-cm^2) results in a very good fill factor for this bandgap.

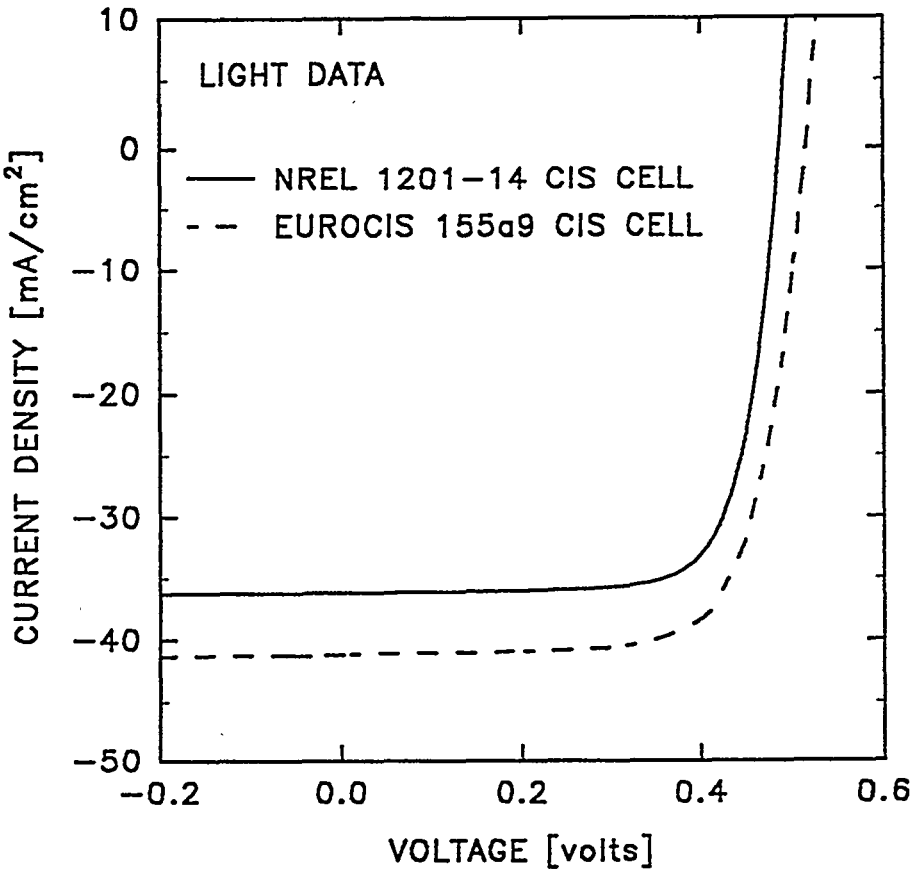

Figure 26. Linear current-voltage characteristics for $CuInSe_2$ cells fabricated by NREL (M1201-14#4) and the EUROCIS collaboration (155a9).

(2) The light and dark curves superimpose within experimental error. (<5 mV difference). The superposition was shown in Fig. 3 at room temperature, but it is seen over the 0-75°C range studied. Other $CuInSe_2$ cells we have examined, even after correction for resistive effects, fail to superimpose by at least 20 mV.

(3) The time-dependent voltage change is smaller than any other thin-film polycrystalline solar cell we have measured (see Table 1). At 2 mV, it is just at the limit of our measurement sensitivity.

A summary of the NREL cell's parameters at four temperatures is given in Table 5. In this case, the values shown for current-density and efficiency are the total area values. The short-circuit current density measured at Colorado State, which did not vary with temperature, was calibrated against the 36.3 mA/cm^2 value from the NREL standardization lab. The bulk hole density deduced from capacitance measurement (Fig. 8) is lower than that seen in many $CuInSe_2$ cells and may be limiting barrier height and hence voltage output.

Table 5: Parameters for NREL $CuInSe_2$ cell M1201-14#4.

	T ≈ 0° C		T ≈ 25° C		T ≈ 50° C		T ≈ 75° C	
	light	dark	light	dark	light	dark	light	dark
V_{oc} [mV]	531	--	485	--	432	--	382	--
J_{sc} [mA/cm^2]	36.3	--	36.3	--	36.3	--	36.3	--
V_{mp} [mV]	443	--	395	--	347	--	308	--
I_{mp} [mA]	13.3	--	13.2	--	13.0	--	12.3	--
ff	0.77	--	0.75	--	0.73	--	0.69	--
η [%] (total area)	14.9	--	13.2	--	11.4	--	9.6	--
A (±0.1)	1.25	1.25	1.2	1.2	1.2	1.15	1.3	1.15
R [Ω-cm^2] (±0.1)	0.16	0.12	0.17	0.19	0.17	0.1	0.2	0.18
r [Ω-cm^2]	>20 K	70 K	>20 K	70 K	>20 K	>30 K	>20 K	>30 K
p [cm^{-3}]	--	$1x10^{16}$	--	$1x10^{16}$	--	--	--	$1x10^{16}$

The forward-current and open-circuit-voltage variation with temperature for the NREL cell is shown in Fig. 27. also shown is the V_{oc} variation for a Cu(In,Ga)Se_2 cell to be discussed in the following section. The forward current was calculated for $J(V) + J_L(V)$ as discussed earlier. The curves are very nearly exponential over a significant range. The dashed lines shown are fits for $R_S \rightarrow 0$, $R_{sh} \rightarrow \infty$. If the room temperature EUROCIS data were overlaid on the T = 25°C curve it would very nearly coincide with the NREL curve at operating voltages and below. Near V_{oc}, however it would lie about 30 mV to the right. The relatively steep slopes in the to part of Fig. 27 correspond to the low A-factor noted above. The open-circuit voltage (lower part of figure) decreases linearly with temperature. Its zero-temperature intercept is slightly above the generally accepted bandgap for $CuInSe_2$.

Cu(In,Ga)Se_2 Cells

Progress with the efficiency of Cu(In, Ga) Se_2 cells has been even more dramatic. Both NREL [4] and EUROCIS [18] have achieved active-area efficiencies above 16%. In the case of NREL, the total-area efficiency has very nearly reached 16%. In both cases, an increase in bandgap of approximately 0.15 eV has been converted to a corresponding increase in open-circuit voltage.

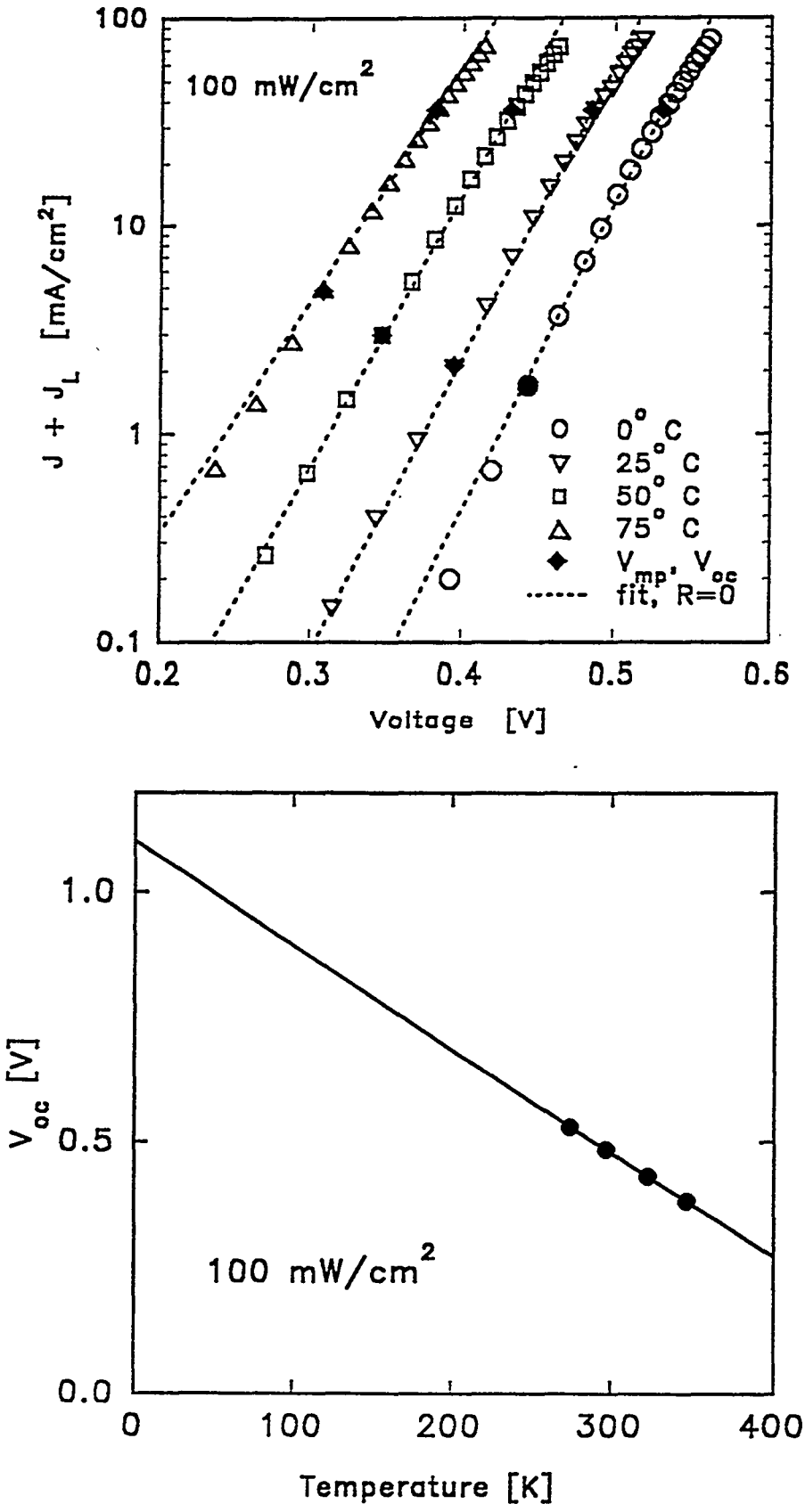

Figure 27. Temperature dependance of forward current (top) and V_{oc} (bottom) for NREL $CuInSe_2$ cell M1201-14#4.

The current-voltage curves for the highest-efficiency Cu(In,Ga) Se_2 cells from NREL and EUROCIS are shown in Fig. 28. both these cells have an area just over 0.4 cm^2. Also shown is a larger area (6 cm^2) NREL cell, which retains many of the features of the smaller cell. Again active-area current density is used for comparative purposes.

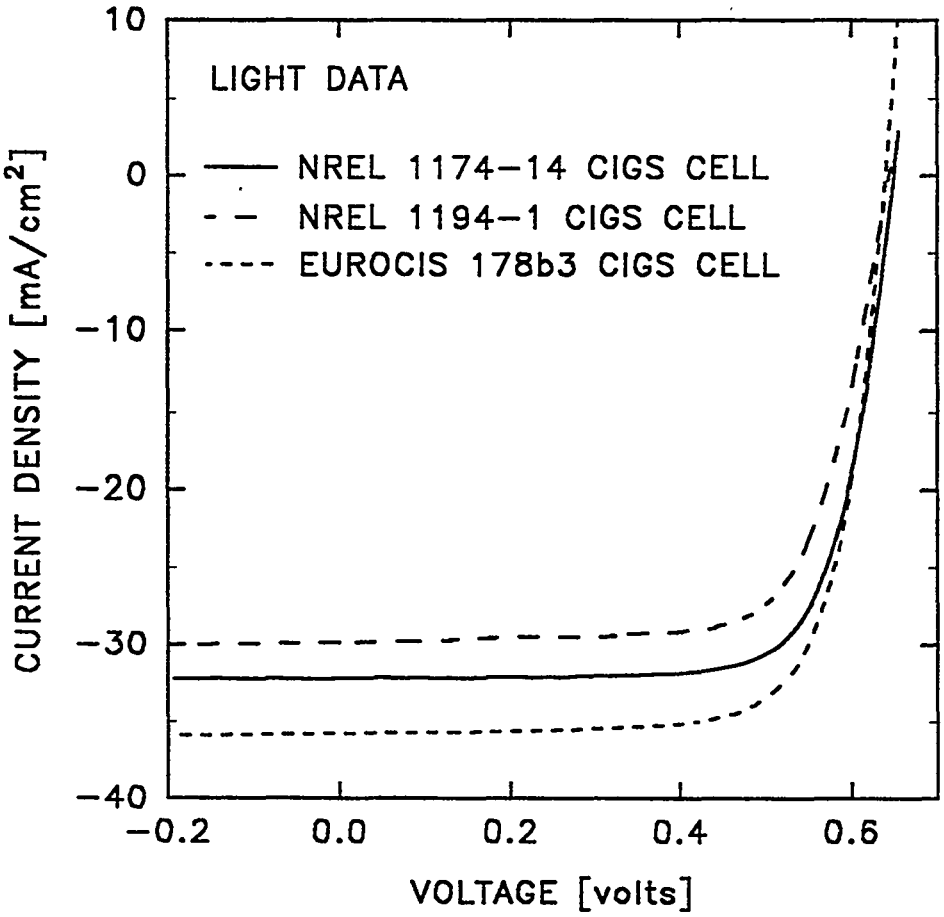

Figure 28. Linear current-voltage characteristics for Cu(In,Ga)Se_2 cells fabricated by NREL (M1174-14, 0.4 cm^2) and the EUROCIS collaboration (178b3, 0.4 cm^3)

The origin of the small current density difference between NREL and EUROCIS is shown clearly in Fig. 29. This figure shows the fraction of photons striking the solar cell that do not contribute to the photocurrent. This fraction is one minus the active area quantum efficiency. The difference, as with the CuIn Se_2 comparison, occurs at short wavelengths and relates to

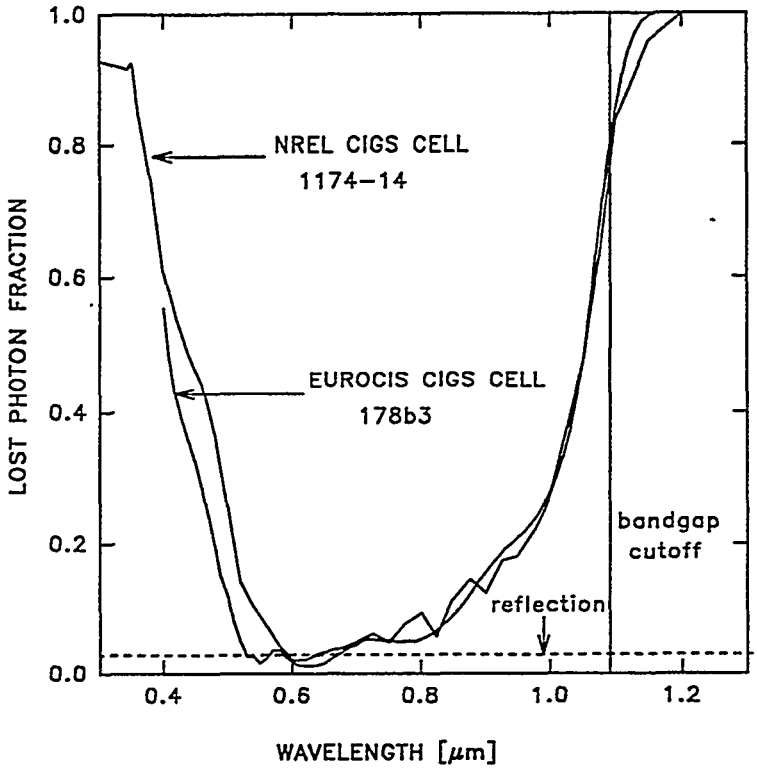

Figure 29. Comparison of photon losses between highest-efficiency NREL and EUROCIS ($Cu(In,Ga)Se_2$ cells.

window absorption, not basic diode parameters. These two cells have an identical bandgap cutoff of 1.14 eV.

The two high-efficiency cells also have nearly identical forward-current characteristics as seen in Fig. 30. The diode quality factor in both cases is about 1.55 and the series resistance is about 0.5 Ω-cm^2. Both these parameters are larger than those in Table 5 for the $CuInSe_2$ cell. The voltage of the NREL cell in Fig. 30 is about 10 mV larger than that of the EUROCIS cell both at V_{oc} and in the operating voltage range. This difference is small enough, however, that it may be due to difference in temperature control between Sweden and Colorado State. When cell 1174-14, for example, was measured by the NREL fabrication lab, the NREL standardization lab, and ours V_{oc} was 645, 649, and 652 mV respectively.

Current-voltage for NREL cell 1174-14 was measured at 0, 25, and 50°C and the basic parameters are summarized in Table 6. Again NREL current measurement was used for

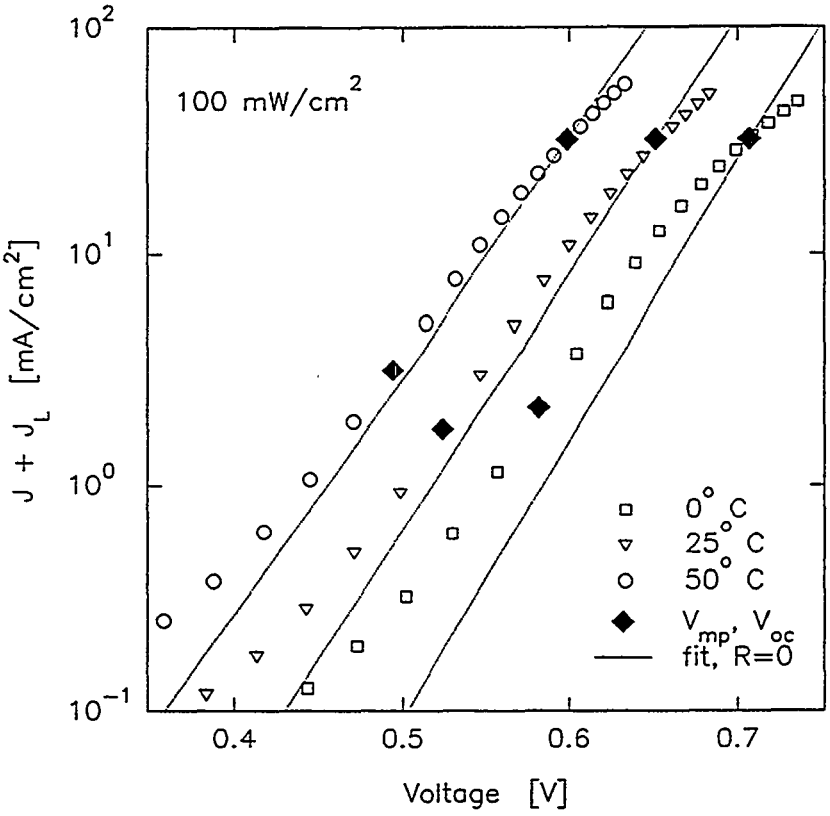

Figure 30. Comparison of forward currents between highest-efficiency NREL and EUROCIS Cu(In,Ga)Se_2 cells.

Table 6: Parameters for NREL Cu(In,Ga)Se_2 cell M1174-14#3

	T ≈ 0° C		T ≈ 25° C		T ≈ 50° C	
	light	dark	light	dark	light	dark
V_{oc} [mV]	707	--	652	--	599	--
ff	0.767	--	0.760	--	0.741	--
η [%] (total area)	17.3	--	15.8	--	14.2	--
A (±0.1)	1.5	1.7	1.5	1.55	1.5	1.5
R [Ω-cm^2] (±0.1)	1.0	1.0	0.6	0.8	0.5	0.5

calibration. The forward-current variation with temperature has a similar slope to the $CuInSe_2$ cell, and the zero temperature intercept of the extrapolated V_{oc} curve (see Fig. 27) is about 0.15 eV larger than that for the $CuInSe_2$ cell, as would be expected from the bandgap difference.

PRESENT STATUS

Comparison to Ideal Cells

To place the current status of thin-film polycrystalline cells in context, we have found it useful to compare the basic parameters achieved to date with those of crystalline cells and those of ideal room-temperature cells. [19] The ideal current density is taken to be the flux of photons in a standard spectrum [3] with energy above the absorber bandgap. V_{oc} is calculated, following Green [20], by assuming that the minimum forward current is the thermionic-emission value and that doping levels approaching degeneracy are practical. There will be some variation in the calculated voltage due to differences in materials parameters among semi-conductors. The ideal fill factor is a simple function of V_{oc} and temperature [21].

Figure 31 shows the highest values of active area current density for two crystalline and three thin-film polycrystalline absorber materials. The variation of ideal values with bandgap puts the

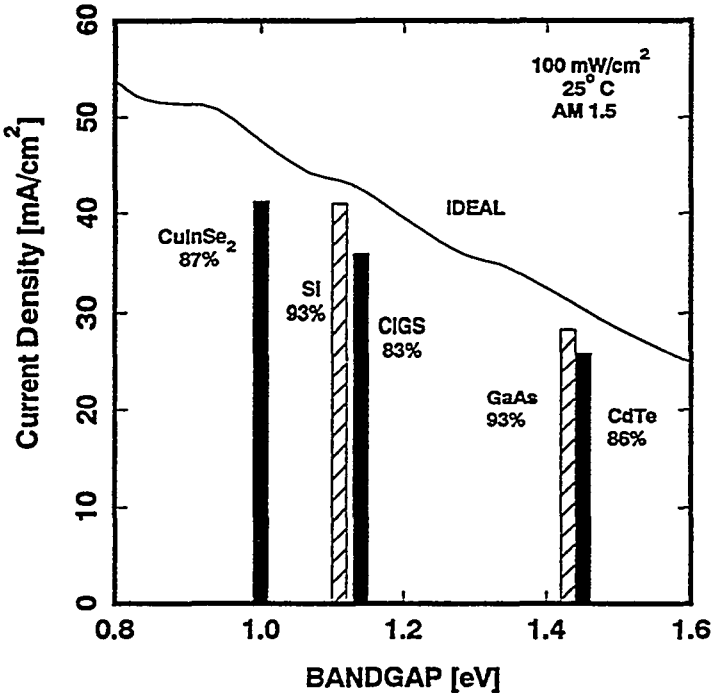

Figure 31. Largest current densities achieved to date for five common solar cell materials. CIGS is Cu(In,Ga)Se_2. Ideal values for 100 mW/cm^2 AM1.5 spectrum shown for comparison.

measured values in context. The percentages indicate the percent of the ideal value that has been achieved. The values for the polycrystalline cells are 6 to 10% lower than the crystalline values. The differences can be explored in more detail through reflection measurement and analysis of the quantum efficiency curves [22]. The differences are (1) the polycrystalline absorbers have smaller diffusion lengths and hence less efficient collection in the red, (2) blue collection is often hampered by the use of CdS window layers on the polycrystalline absorbers, and (3) the development of AR coatings for polycrystalline cells is somewhat less developed.

Fig. 32 shows the open-circuit voltage values achieved compared to the average of the calculated range. Here the difference between single-crystal and polycrystalline thin-film cells is somewhat greater ($\sim 15\%$). The primary difference is that the forward current in even the best polycrystalline cells is at least one order of magnitude larger than single-crystal values under operating conditions. The forward-current mechanism for the polycrystalline cells is clearly not thermionic emission. Diode quality factors under illumination are typically near 2.0 for the best CdTe cells and near 1.5 for high-efficiency $CuInSe_2$ and CIGS cells.

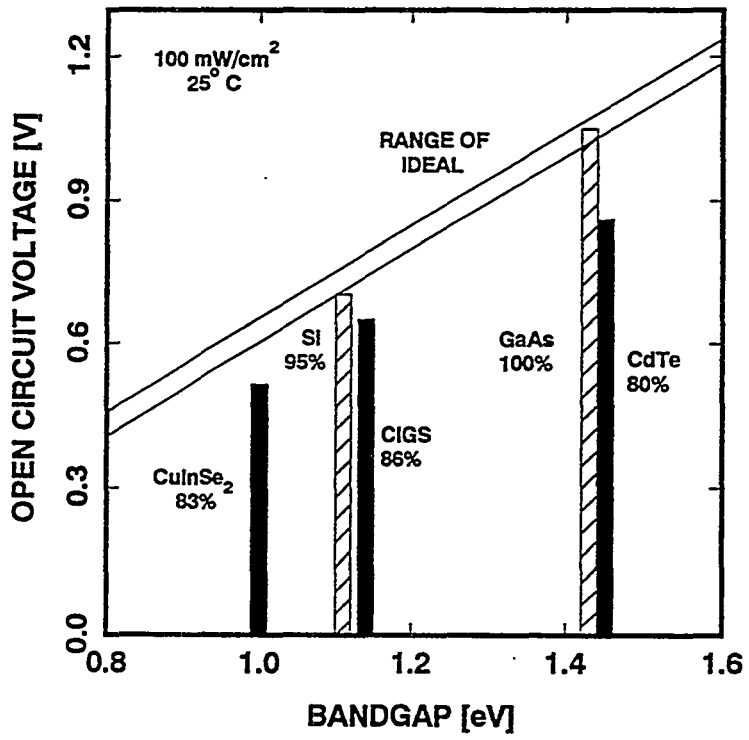

Figure 32. Largest voltages achieved to date for AM1.5 conditions. Range of ideal values shown for reference.

Fig. 33 gives the fill factor comparison. Here also the polycrystalline cells have lower values relative to the ideal. The differences are about 10% The largest decrease in fill factor is due to the larger diode quality factors mentioned above. The largest diode quality factor values are those of CdTe, and it in fact typically has the smallest fill factor in comparison to the ideal. Polycrystalline thin-film cells also suffer somewhat in fill factor because they tend to have larger series resistance than crystalline cells. Finally, there is a second-order limitation on fill factors when the voltage is reduced relative to the bandgap.

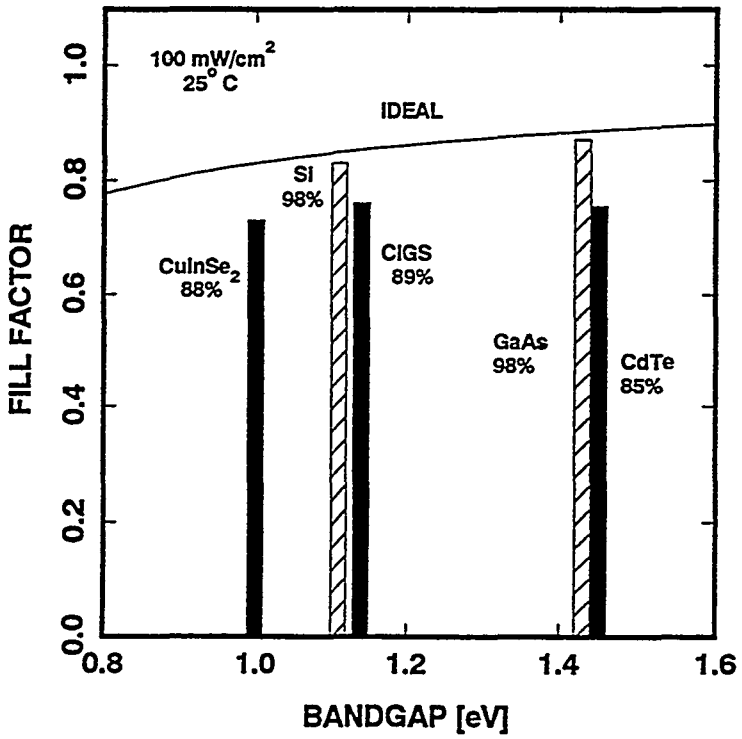

Figure 33. Largest fill factors achieved to date. Ideal curve is relative to the bandgap and assumes a near-ideal voltage has been achieved.

Figs. 31-33 show that the individual polycrystalline parameters are all reasonably respectable. The cumulative differences lead to efficiency values about two-thirds those of Si and GaAs, as shown in Fig. 34. This differential, however, may well be acceptable in the context of fabrication economics. Furthermore, the fractional differential in efficiency between crystalline and polycrystalline thin-film cells has been steadily narrowing during the past decade. This trend can be expected to continue, since there are a number of small improvements which can be made to the polycrystalline cells even without major breakthroughs.

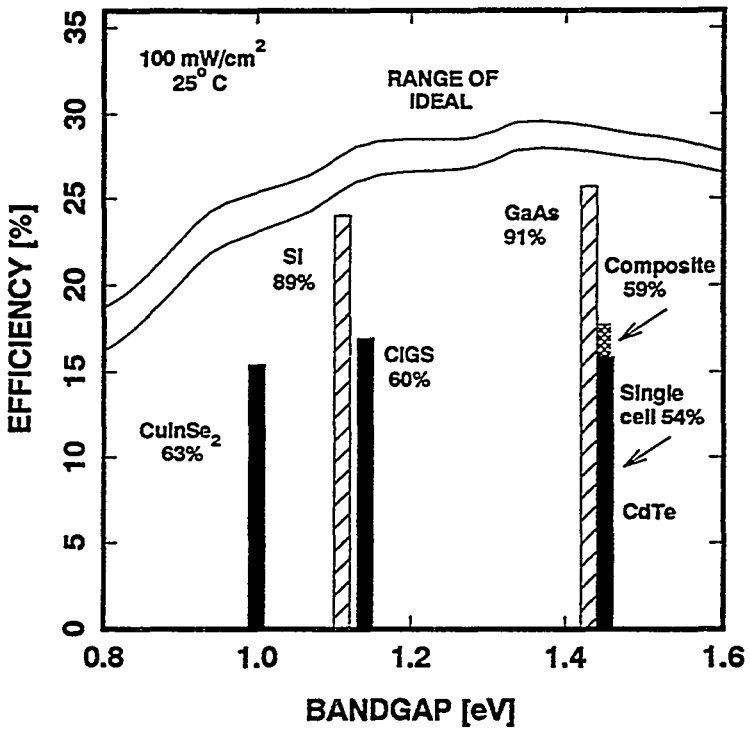

Figure 34. Highest efficiencies achieved by five types of solar cells. Both single-cell and composite values are shown for CdTe.

For the CdTe cells there is a significant difference between the highest efficiency achieved in a single cell and the composite value when the highest current and voltage from two different cells are combined. Thus, both are shown in Fig. 34. For the other types of cells, the differences between composite and single cell efficiencies are minimal.

Forward-Current Model

A longstanding difficulty with understanding thin-film polycrystalline cells has been the lack of a forward-current model that is consistent with experimental results when temperature and illumination are varied. A common experimental observation that is not easily explained is a diode quality factor that varies with temperature and/or illumination intensity [23, 24], and in some cases is larger than the upper limit of 2 predicted by the Shockley-Read-Hall (SCR) recombination model. The modeling problems likely result from the polycrystalline nature of the materials. They may be compounded by the time-dependent effects discussed above which appear to have different magnitudes of extraneous-state population at different temperatures even when the same time sequence is used in the measurements.

Fig. 35 shows four of the current mechanisms that may be operative in thin-film polycrystalline cells. The diagram assumes that the grain-boundary region is depleted, but that the grain-

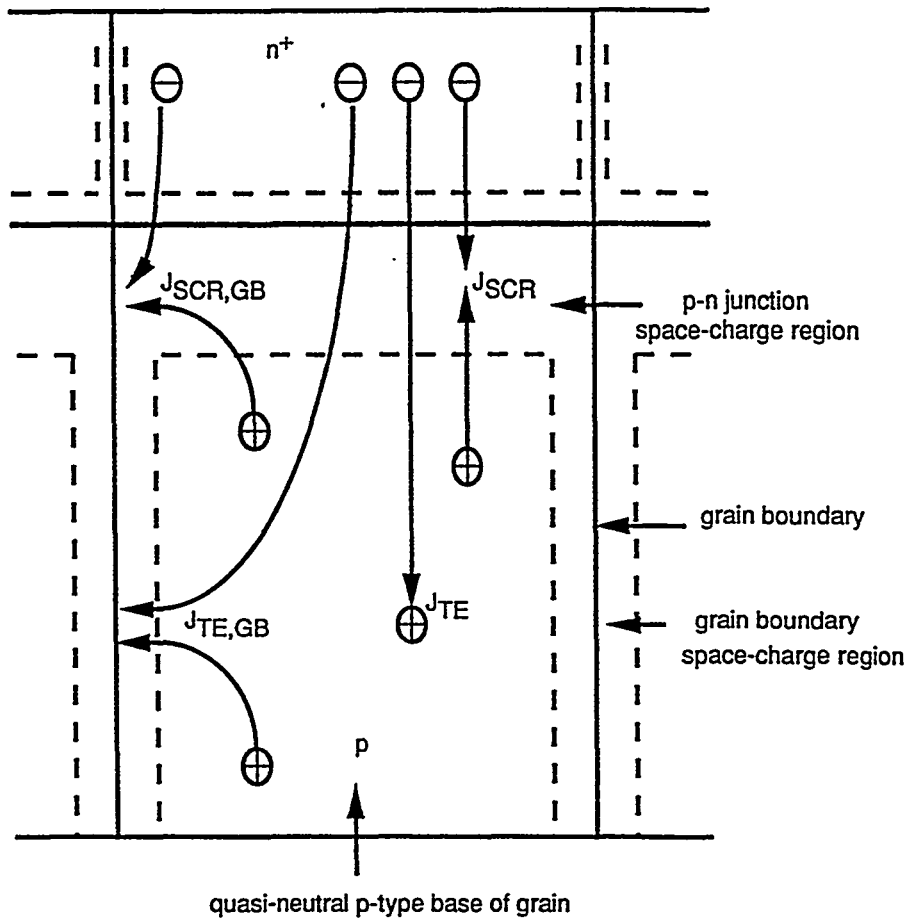

Figure 35. Forward-current mechanisms for polycrystalline diodes. (TE thermionic emission, SCR Shockley-Read-Hall recombination, GB grain boundaries)

boundary barrier is smaller than the junction barrier. The thermionic-emission and SCR-recombination paths are independent of the polycrystallinity. Grain-boundary enhanced recombination in the junction regions ($J_{SCR,GB}$), however, can be dominant over a voltage range that varies with temperature. The fourth mechanism shown is believed to be smaller and probably negligible.

Fig. 36 shows the dark data for NREL $CuInSe_2$ cell M1201 at four temperatures (the triangle data appears to have been recorded at a slightly higher temperature than intended). The hole density is determined independently, and diffusion length L_n, bulk trap density $N_{t,bulk}$, and trap

energy E_t - E_i are used as fitting parameters. In this case, grain boundary traps $N_{t,gb}$ are not required for a reasonably good fit. Additionally, illumination effects are not an issue for this

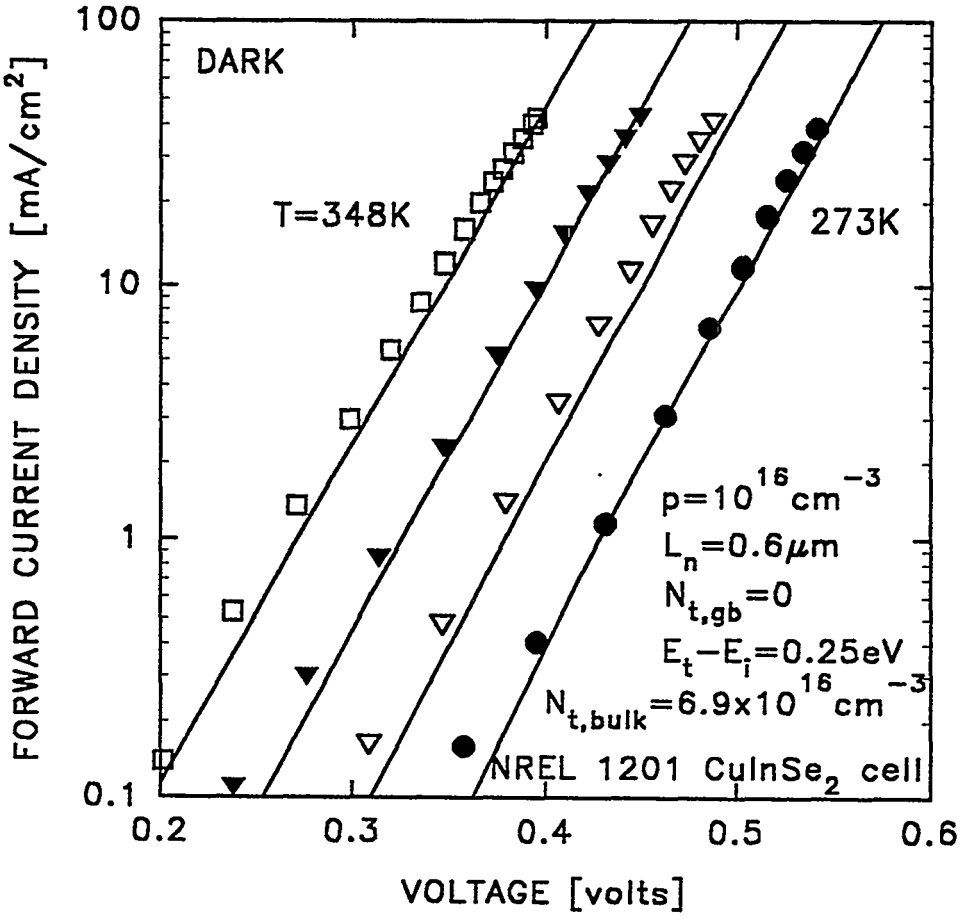

Figure 36. Model fit to forward/current density for NREL cell M1201-14#4.

cell since it shows excellent light-dark superposition. For most other $CuInSe_2$ cells, however, the $J_{SCR,GB}$ term is significant, and a value of $N_{t,gb}$ of approximately 10^{12} cm^{-2} is required. Such fits appear to be successful for cells fabricated at Siemens and IEC, but it is not yet clear whether the mechanisms depicted in Fig. 35 are sufficient for all thin-film polycrystalline cells. In particular, we need to leave open the possibility of carrier transport along a grain boundary by a hopping mechanism.

RECOMMENDATIONS

The first recommendation is to continue to refine loss-mechanism analysis techniques and to apply these techniques more generally to solar cells being fabricated throughout the community. Increased use of quantitative loss separation analysis meshes nicely with the increasing trend for cell-fabrication groups to make a series of test cells on a common substrate with a systematic variation in a single fabrication parameter.

The second recommendation is to extend single-cell analysis to the module level. Many of the techniques are still operable, but there are additional challenges related to temperature and illumination uniformity, less-optimal cell geometries, complications in process control, multiple cells in series, and problems with contacts between cells. Successful module analysis and feedback probably requires even more cooperation throughout the community than cell analysis.

The third recommendation is enhanced data exchange between laboratories. The network hardware is in place nationwide, and in some cases is used extensively. There are frequent challenges, however, in working out formats and protocols, there is a continuing need for sensitivity in distributing credit for results, and there are local needs for additional investment in hardware or expertise.

In general, recent developments in producing and understanding polycrystalline thin-film cells point to a high probability for a major impact on power production. It would appear to be a wise investment to continue to promote progress in both the production and the understanding.

COMMUNICATIONS

Publications

1. "Analysis of Apparent Quantum Efficiency," Solar Cells **29**, 39 (1990). J.R. Sites, H. Tavakolian, and R.A. Sasala.

2. "Individual Losses in Thin-Film CdTe Solar Cells," Proc. 21st IEEE Photovoltaics Specialists Conf., Orlando, 1990, p. 556. H. Tavakolian and J.R. Sites.

3. "Annealing Effects on Individual Loss Mechanisms in $CuInSe_2$ Solar Cells." Solar Cells **30**, 101 (1990). R.A. Sasala and J.R. Sites.

4. "Junction Analysis of Selenized $CuInSe_2$ Solar Cells," Proc. 22nd IEEE Photovoltaics Specialists Conf., Las Vegas, 1991, p. 930. X.X. Liu, R.A. Sasala, and J.R. Sites.

5. "Comparative Analysis of Recent High-Efficiency CdTe Solar Cells," Int. J. Solar Energy **12**, 17 (1992). R.A. Sasala, X.X. Liu, and J.R. Sites.

6. "Transient Voltage of Thin-Film Polycrystalline Solar Cells" AIP Conf. Proc. 268, **218** (1992). R.A. Sasala and J.R. Sites.

7. "Trade-off Between Collection Efficiency and Open-Circuit Voltage," Proc. 23rd IEEE Photovoltaic Specialists Conf., Louisville, 1993, p. 501. X.X. Liu and J.R. Sites.

8. "Time-Dependent Voltage in $CuInSe_2$ and CdTe Solar Cells," Proc. 23rd IEEE Photovoltaics Specialists Conf., Louisville, 1993, p. 543. R.A. Sasala and J.R. Sites.

9. "Analysis of Losses in High-Efficiency CdTe Cells," Proc. 23rd Photovoltaics Specialists Conf., Louisville, 1993. p. 405. X.X. Liu, I.L. Eisgruber, and J.R. Sites.

10. "Variation of Solar-Cell Collection Efficiency with Depletion Width," J. Appl Phys. **75**, 572 (1994).

11. "Status of Polycrystalline Thin-Film Solar Cells," AIP Conf. Proc. xx, xxx (1994). I.L. Eisgruber and J.R. Sites.

Ph.D. Thesis

1. "Multi-Decade Time-Dependent Voltage of Polycrystalline Thin-Film Solar Cells." R.A. Sasala, Colorado State University, Dec. 1993, unpublished.

Talks

1.	PVSC-21	Orlando FL	Sites	May 1990
2.	PVAR&D-10	Denver CO	Sites	October 1990
3.	Solarex	Newtown PA	Sites	February 1991
4.	Solar Energy Res. Inst.	Golden CO	Sites	August 1991
5.	PVSC-22	Las Vegas NV	Sites	November 1991
6.	Colorado Seed Growers	Estes Park CO	Sites	December 1991
7.	Colorado State Univ.	Ft. Collins CO	Sites	January 1992
8.	Colorado School of Mines	Golden CO	Sites	April 1992
9.	PVAR&D-11	Denver CO	Sites	May 1992
10.	Jilin University	Changchun China	Sites	August 1992
11.	Performance/Reliability Workshop	Denver CO	Sites	September 1992
12.	Materials Res. Soc.	San Francisco CA	Sasala	April 1993
13.	PVSC-23	Louisville KY	Sites	May 1993
14.	NASA Lewis	Cleveland OH	Sites	August 1993
15.	Solar Cells, Inc.	Toledo OH	Sites	August 1993

Specific Cell Reports

Date	Cell Type	Origin	Cell Number	Sent To
8/10/90	CIS	IEC	3190113-12	Ullal
12/6/90	CIS	ISET	489B	Ullal
6/15/91	CdTe	Ph.Energy Ametek	3 91A6-2	Ullal
8/12/91	CdTe	USF BP	5-16-8-1 5-10-17-1 "13.2%"	Ullal
8/20/91	CdTe	USF	5-16-8-1	Zweibel
9/3,10/91	CdTe	Ph.Energy	952D4	Zweibel
11/15,21,22/91	CdTe	USF	11-4-8A	Ullal
1/10/92	CIGS	Boeing	1460AA	Ullal
2/24/92	CdTe	SCI	A749A#15	Ullal
4/18/92	CIGS	Boeing	1490AD	Ullal
4/15/92	CIS CIGS	EUROCIS EUROCIS	"14.8%" "14.6%"	Ullal
4/29/92	CIS	NREL	S193-3#1	Tuttle
6/10/92	CdTe	GIT	1-1, 2-4	von Roedern
6/10/92	CdTe	USF	4-23A-14#C, -1#A	Zweibel
6/30/92	CdTe	USF	4-23A-14#C, -1#B	Ullal
7/10/92	CdTe	USF	5-1A-12ABC 5 - 1 9 B - 19ABC 6-1B-1-B	von Roedern

7/17/92	CdTe	USF	5-1A-12ABC 5 - 1 9 B - 19ABC 6-1B-1-B	von Roedern
7/27/92	CdTe CdTe CIS	NREL Battelle EUROCIS	S45-11-2#2 S8ba 63#2,69#5	Ullal
9/2/92	CIS	ISET	R297B (4 cells)	Basol
10/21/92	CdTe	USF	5-16-8-1	Zweibel
11/16/92	CdTe	Toledo	SC275-11	Ullal
12/11/92	CdTe	USF	5-19B-10A	von Roedern
2/18/93	CIGS	NREL	5319-4-5	von Roedern
4/12/93	CIS	NREL	5339-4 (6 cells)	von Roedern
5/21/93	CdTe	GIT	2-3, 5-3; 5-6	von Roedern
6/7/93	CIS CIGS	NREL/Stgt. NREL	U110892/1-6 312, 343, 336,350	Tuttle
6/18/93	CIS CIGS	EPV/NREL EUROCIS	2-4 173 b3	Ullal
7/7/93	CIGS CdTe	NREL SCI	3423-14#5 8117E4#33	Ullal
7/20/93	CIGS	NREL	M1174-14#3	Ullal
9/2/93	CIGS	NREL	M1194-1	Tuttle
9/6/93	CIGS	Boeing	1570-A14	Ullal
10/3/93	CIS	NREL	C202#7	Tuttle
12/8/93	CIS	NREL	M1201-14#4	Gabor

REFERENCES

1. X.X. Liu and J.R. Sites, "Trade-off Between Collection Efficiency and Open-Circuit Voltage," Proc. 23rd IEEE Photovoltaics Specialists Conf., Louisville, 1993, p. 501.

2. X.X. Liu and J.R. Sites, "Variation of Solar-Cell Collection Efficiency with Depletion Width," J. Appl. Phys. **75**, 572 (1994).

3. R. Hulstrom, R. Bird, and C. Riordan; "Spectral Solar Irradiance Data Sets for Selected Terrestrial Conditions." (table 2b), Solar Cells **15**, 365 (1985).

4. A.M. Gabor, J.R. Tuttle, D.S. Albin, A.L. Tennant, M.A. Contreras, R. Noufi, and A.M. Hermann, "High Efficiency Polycrystalline Cu(In,Ga)Se_2-Based Solar Cells." AIP Conf. Proc.,to be published.

5. R.A. Sasala, X.X. Liu, and J.R. Sites, "Comparative Analysis of Recent High-Efficiency CdTe Solar Cells," Int. J. Solar Energy **12**, 17 (1992).

6. D.A. Fardig, "Characterization of CdTe/CdS Solar Cells," M.S. Thesis, University of Delaware, June 1991 (unpublished).

7. D.A. Fardig and J.E. Phillips, "Characterization of CdTe/CdS Solar Cells," Proc. 22nd IEEE Photovoltaics Specialists Conf., Las Vegas, 1991, p. 1146.

8. P.H. Mauk, H. Tavakolian, and J.R. Sites, "Interpretation of Thin-Film Polycrystalline Capacitance," IEEE Trans. **EO-37**, 422 (1990).

9. R.E. Hollingsworth and J.R. Sites, "Annealing Temperature Effects on $CuInSe_2$/CdS Solar Cells," Solar Cells **16**, 457 (1986).

10. R.A. Sasala and J.R. Sites, "Annealing Effects on Individual Loss Mechanisms in $CuInSe_2$ Solar Cells," Solar Cells **30**, 101 (1991).

11. R.J. Matson, C.R. Herrington, R. Noufi, and R.C. Powell, "EBIC Studies of Junction Formation and the Role of Oxygen in Thin-Film CdS/$CuInSe_2$ Solar Cells." Proc. 18th IEEE Photovoltaics Specialists Conf., Las Vegas, 1985, p. 1648.

12. R.A. Sasala and J.R. Sites, "Transient Voltage of Thin-Film Polycrystalline Solar Cells," AIP Conf. Proc. **268**, 218 (1992).

13. R.A. Sasala and J.R Sites, "Time Dependent Voltage in $CuInSe_2$ and CdTe Solar Cells," Proc. 23rd IEEE Photovoltaics Specialists Conf., Louisville, 1993, p. 543.

14. R.A. Sasala, "Multi-Decade Time-Dependent Voltage of Polycrystalline Thin-Film Solar Cells," Ph.D. Thesis, Colorado State University. Dec. 1993, unpublished.

15. T.L. Chu, S.S. Chu, J. Britt, C. Ferekides, C. Wang, C.Q. Wu, and H.S. Ullal, "14.6% Efficiency Thin Film Cadmium Telluride Solar Cells," IEEE Electron Dev. Lett **13**, 303 (1992)

16. C. Ferekides, J. Britt, X. May, and L. Killian, "High Efficiency CdTe Solar Cells by Close Spaced Sublimation," Proc. 23rd IEEE Photovoltaics Specialists Conf., Louisville, 1993, p. 389.

17. H. Tavakolian and J.R. Sites, "Individual Losses in Thin-Film CdTe Solar Cells," Proc. 21st IEEE Photovoltaics Specialists Conf., Orlando, 1990, p. 556.

18. J. Hedström, H. Ohlsén, M. Bodegärd, A. Kylner, L. Stolt, D. Hariskos, M. Ruckh, and H.-W. Schock, "Zn0/CdS/Cu(In, Ga)Se_2 Thin Film Solar Cells with Improved Performance," Proc. 23rd IEEE Photovoltaics Specialists Conf., Louisville, 1993, p. 364.

19. I.L. Eisgruber and J.R. Sites, "Status of Polycrystalline Thin-Film Solar Cells," AIP conf. Proc. xxx, xxx (1994).

20. M.A. Green, Solar Cells: *Operating Principles, Technology, and Systems Applications* (Prentice-Hall, Englewood Cliffs, NJ, 1982), p. 76.

21. *Ibid.*, p. 80

22. J.R. Sites, H. Tavakolian, and R.A. Sasala, "Analysis of Apparent Quantum Efficiency," Solar Cells **29**, 39 (1990).

23. X.X. Liu, R.A. Sasala, and J.R. Sites, "Junction Analysis of Selenized $CuInSe_2$ Solar Cells," Proc. 22nd IEEE Photovoltaics Specialists Conf., Las Vegas, 1991, p. 930.

24. X.X. Liu, I.L. Eisgruber, and J.R. Sites, "Analysis of Losses in High-Efficiency CdTe Cells." Proc. 23rd Photovoltaics Specialists Conf., Louisville, 1993, p. 405.

REPORT DOCUMENTATION PAGE

Form Approved
OMB NO. 0704-0188

1. AGENCY USE ONLY (Leave blank)	2. REPORT DATE	3. REPORT TYPE AND DATES COVERED
	July 1994	Final Subcontract Report — 1 April 1990 - 30 November 1993

4. TITLE AND SUBTITLE

Role of Polycrystallinity in CdTe and $CuInSe_2$ Photovoltaic Cells

5. FUNDING NUMBERS

C: XC-0-10046-1

TA: PV431101

6. AUTHOR(S)

J. R. Sites

7. PERFORMING ORGANIZATION NAME(S) AND ADDRESS(ES)

Colorado State University
Department of Physics
Fort Collins, CO 80523

8. PERFORMING ORGANIZATION REPORT NUMBER

9. SPONSORING/MONITORING AGENCY NAME(S) AND ADDRESS(ES)

National Renewable Energy Laboratory
1617 Cole Blvd.
Golden, CO 80401-3393

10. SPONSORING/MONITORING AGENCY REPORT NUMBER

TP-451-7047

DE94011849

11. SUPPLEMENTARY NOTES

NREL Technical Monitor: B. von Roedern

12a. DISTRIBUTION/AVAILABILITY STATEMENT

12b. DISTRIBUTION CODE

UC-273

13. ABSTRACT *(Maximum 200 words)*

The report describes the exploration of several aspects of the role of polycrystallinity in the operation of CdTe, $CuInSe_2$, and $Cu(In,Ga)Se_2$ solar cells. The work included the refinement of several analytical techniques, the documentation and understanding o time-dependent voltage effects, the analysis of a large number of inidividual cells, and significant progress toward developing a viabl current-voltage model. This work was integral to the doctoral training of four students and was greatly assisted by several active collaborations within the polycrystalline thin-film solar cell community.

14. SUBJECT TERMS

cadmium telluride ; copper indium diselenide ; polycrystalline thin film s; polycrystallinity ; photovoltaics ; solar cells

15. NUMBER OF PAGES
60

16. PRICE CODE
A04

17. SECURITY CLASSIFICATION OF REPORT	18. SECURITY CLASSIFICATION OF THIS PAGE	19. SECURITY CLASSIFICATION OF ABSTRACT	20. LIMITATION OF ABSTRACT
Unclassified	Unclassified	Unclassified	UL